Orthopyroxene Stability within Kimberlite Magma: An Experimental Investigation

by
Daniel A. B. Jacobs

Thesis presented in partial fulfilment of the requirements for the degree Master of Science at the University of Stellenbosch

Supervisor: Prof. Gary Stevens
Co-supervisor: Prof. Anton P. le Roex
Faculty of Science
Department of Earth Sciences

March 2012

Declaration

By submitting this thesis/dissertation electronically, I declare that the entirety of the work contained therein is my own, original work, that I am the sole author thereof (save to the extent explicitly otherwise stated), that reproduction and publication thereof by Stellenbosch University will not infringe any third party rights and that I have not previously in its entirety or in part submitted it for obtaining any qualification.

Signature: _____

February 2012

Abstract

The common presence of large volumes of coarse-grained olivine in kimberlite magmas has been proposed to attest to the volume of mantle xenolith material that has been disaggregated during the ascent of the magma. Orthopyroxene should constitute 10-50 vol% of mantle xenoliths in kimberlites, some of which must be disaggregated into the kimberlite, yet it is typically absent. This work tests the stability of orthopyroxene in ascending kimberlite magma by conducting experiments at pressures between 2.0 and 3.5 GPa and temperatures between 1100 and 1300°C. The starting material consisted of natural hypabyssal kimberlite that is close in composition to primary group I kimberlite magma with 5wt% orthopyroxene sourced from a natural peridotite added. At higher temperatures and pressures it is seen that orthopyroxene quantities exceed that of the starting material, but at lower temperatures and pressures it is absent. These results indicate that orthopyroxene is not stable in the magma composition investigated within the shallower part of the sub-continental lithospheric mantle. Based on increased olivine volumes in the experiments where orthopyroxene disappeared, as well as textural relationships between olivine and orthopyroxene, it is found that orthopyroxene dissolution is incongruent along the reaction $Mg_2Si_2O_6$ (opx) = Mg_2SiO_4 (ol) + SiO_2 (in the liquid). It is concluded that this reaction leads to a maximum addition of 5.5 vol% peritectic olivine to the kimberlite as it ascends through the depths equivalent to a pressure window of 2.0 to 3.5 GPa.

Uittreksel

Die algemene teenwoordigheid van groot volumes grof-gegranuleerde olivien in kimberliet magmas is voorgestel om te getuig van die volume mantel xenoliet materiaal wat tydens die styging van die magma disaggregeer het. Ortopirokseen behoort 10-50vol% van mantel xenoliete op te maak in kimberliet, waarvan n gedeelte in die kimberliet gedisaggregeer behoort te wees, maar tog is dit gewoonlik afwesig. Hierdie studie toets die stabiliteit van ortopirokseen deur die uitvoer van eksperimente by drukke tussen 2.0 en 3.5 GPa en temperature tussen 1100 en 1300°C. Die begin material het bestaan uit natuurlike hipabissale kimberliet, naby in samestelling aan primêre groep I kimberliet magma met 5wt% ortopirokseen, verkry van ‘n natuurlike peridotiet. By hoër temperature en drukke word gesien dat die hoeveelhede ortopirokseen groter is as in die oorspronklike begin material, maar teen laer temperature en drukke word dit gevind dat ortopirokseen afwesig is. Hierdie resultate dui daarop dat ortopirokseen nie stabiel is in die magma samestelling ondersoek binne die vlakker deel van die sub-kontinentale lithosferiese mantle nie. Op grond van die verhoogde olivien volumes teen laer temperature en drukke asook tekstuur verhoudings tussen olivien en ortopirokseen, word gevind dat die versmelting van ortopirokseen inkongruent is volgens die reaksie $Mg_2Si_2O_6$ (opx) = Mg_2SiO_4 (ol) + SiO_2 (in die vloeistof). Die gevolgtrekking word bereik dat hierdie reaksie lei tot 'n maksimum toevoeging van 5.5 vol% peritektiese olivien tot die kimberliet soos dit styg deur die dieptes gelykstaande aan ’n druk venster van 2.0 tot 3.5 GPa.

Acknowledgements

The research for this study was funded by the South African National Research Foundation (NRF) in the form of grant funding to Professor G Stevens via the SARChI programme and an MSc Bursary to D. Jacobs.

Prologue

The work contained in this thesis was performed independently by myself under the guidance of my supervisor, Prof Gary Stevens (Stellenbosch University), and co-supervisor, Prof Anton le Roex (University of Cape Town). Prof Gary Stevens provided insight and advice on experimental technique and the analysis of phases, whilst Prof Anton le Roex's kimberlite expertise and knowledge of kimberlite petrogenesis provided guidance in those areas. Both Prof Stevens and Prof le Roex provided valuable guidance on the interpretation of the results obtained through this study. In addition to this, Prof le Roex provided the kimberlite used in the starting material.

A manuscript in very similar form to this thesis is currently under review at Contributions to Mineralogy and Petrology.

Table of contents

Introduction

Kimberlites form from ultramafic magmas that occur as eruptive rocks or as typically dyke-shaped intrusions into the crust. They are best known for being the primary source of diamonds and other xenolithic mantle material. Both the unusual chemistry of these magmas and the economic value of diamonds has resulted in extensive investigation of the origins of these rocks (e.g. Arndt et al. 2010; Becker and le Roex 2006; Canil and Bellis 2008; Dalton and Presnall 1998; Edgar and Charbonneau 1993; Eggler and Wendlandt 1979; Girnis et al. 1995; Harris et al. 2004; Keshav et al. 2005; Kopylova et al. 2007; Mitchell 2004; Price et al. 2000; Ringwood et al. 1992; Ryabchikov and Girnis 2005; Wyllie 1980). Collectively, this body of work illustrates that kimberlite petrogenesis is all but simple. In part, this complexity results from their ability to entrain and potentially digest significant volumes of xenolithic material gathered from the mantle and crustal rocks the magma must traverse as it ascends into the upper crust. As kimberlite occurrences are concentrated within the ancient cratons, the xenoliths they exhume provide a unique insight into the sub-continental lithospheric mantle and have been very important in understanding the complexity that exists within the sub-continental lithosphere (Dawson 1980; McDonald and Viljoen 2006). Further uncertainty surrounds the concentrations of volatiles native to primary kimberlite melt. This results from the fact that kimberlite magmas very likely arise at a pressure in excess of the relevant 2nd critical point and become volatile oversaturated during ascent. Rising H_2O and CO_2 activity and, ultimately fluid saturation, drives hydration and carbonation reaction in the magma. Additionally, serpentinization and carbonation of kimberlites also occurs due to interaction with crustally derived fluids (Mitchell 1986, Sparks et al. 2006). Consequently, gauging the volatile content and composition of kimberlite magmas is very problematic.

As a consequence of the substantial body of research on kimberlites, several aspects of their petrogenesis are reasonably well constrained, e.g. their mantle origin, the effects of crustal contamination on their chemistry and their post emplacement alteration. Other aspects of kimberlite petrogenesis remain largely unresolved. One such issue is the composition of primary kimberlite magma. The characteristics of natural kimberlite occurrences, however, do not allow this question to be easily answered. Part of the reason for this is the entrainment, hydration and carbonation issues discussed above, with fractional crystallization from the low viscosity magmas (e.g. le Roex et al., 2003; Harris et al., 2004; Becker & le Roex, 2006) and the lack of quenched kimberlitic glasses (Mitchell, 2008) also being problematic. Experimental studies possibly have strong potential to address this issue and such studies are discussed below.

An additional issue related to primary magma and melt composition of kimberlites is the interpretation that much of the olivine that occurs within kimberlites represents xenocrystic material derived from the disaggregation of mantle xenoliths. This xenocrystic olivine commonly occurs as a population of large rounded to sub-rounded grains, referred to as macrocrystic (Clement 1982; Mitchell 1986). In contrast, phenocrystic olivine occurs in the groundmass in the form of smaller often euhedral-to-subhedral grains. Studies of mantle xenoliths within kimberlites indicates that a substantial fraction of these consist of orthopyroxene (10-50%; Mitchell 2008). Unlike olivine, this orthopyroxene component is effectively absent from hypabyssal kimberlite (Arndt et al. 2010; Mitchell 2008), and is only found as minor inclusions inside olivine and very rarely as highly altered xenocrystal fragments (Kamenetsky et al., 2009). Although hypabyssal kimberlite cannot be taken as a direct representative of the primary kimberlite composition (Mitchell ,2008), it is arguably the closest proxy available, and as such, the lack of orthopyroxene therein either indicates the instability of orthopyroxene within kimberlitic magma or that the interpretation of the origin of macrocrystic olivine is incorrect.

This study aims to investigate orthopyroxene stability in kimberlite magma through experimentally replicating a segment of the kimberlite ascent path. By melting natural kimberlite seeded with a peridotitic mineral suite, including orthopyroxene, under upper mantle conditions, this work simulates an ascending kimberlite as it interacts with peridotite. This allows investigating the behaviour of entrained orthopyroxene as a function of pressure and temperature. If it can be demonstrated that the magma effectively digests orthopyroxene, the implications will be both that the magma compositions recorded in aphanitic kimberlites are more SiO_2-rich than those that existed prior to orthopyroxene digestion and that much of the euhedral olivine may have formed from incongruent melting of orthopyroxene in the magma. Consequently, some fraction of this euhedral olivine should not be regarded as material that crystallized directly from the magma.

Previous studies

Previous investigations relevant to OPX stability in kimberlite magmas

Several previous studies have concluded that orthopyroxene is likely to have limited stability in typical kimberlite magma compositions (e.g. Le Roex et al., 2003; Mitchell, 2006; Kopylova et al. 2007; Kamenetsky et al., 2009; Arndt et al. 2010), but as yet this has not been confirmed through experimental investigation. The experimental work of Eggler (1973) shows that orthopyroxene is stable in a fluid with high CO_2 contents ($CO_2/[CO_2+H_2O]>0.4$) but that it breaks down at higher H_2O contents by, melting incongruently to form olivine and a more SiO_2 rich melt. Additionally, Luth (2009) suggests that orthopyroxene is not stable in a melt with low SiO_2 activity (also supported by e.g. Mitchell, 1973; Mitchell, 2008; Kopylova et al., 2007), and that decreasing pressure lowers the SiO_2 activity in a liquid coexisting with forsterite and enstatite,

driving the reaction, $Mg_2Si_2O_6$ (opx) = Mg_2SiO_4 (ol) + SiO_2 (in the liquid), towards the production of olivine. This type of pressure related dissolution corresponds well with the notion that orthopyroxene was dissolved into the kimberlitic magma during ascent to surface (Brett et al., 2009; Kamenetsky et al., 2009). Based on the observation of monomineralic dunitic nodules in kimberlites consisting of olivine with variable Mg#, Arndt et al. (2010) propose a different dissolution mechanism whereby orthopyroxene is removed from xenoliths prior to entrainment. They suggest that a SiO_2-poor protokimberlitic fluid, rich in CO_2-H_2O-Cl, undergoes in-situ reaction with mantle peridotites such as lherzolite and harzburgite to remove the more soluble components such as pyroxene and garnet, and producing dunite. The probable presence of such a chloride-carbonate fluid in the mantle has been argued by Kamenetsky et al. (2004), Kamenetsky et al. (2007) and Kamenetsky et al. (2009), who have recognized the strong metasomatic effect of such a liquid. The theories above are based on observations in natural rocks. This study will experimentally test the idea that orthopyroxene is not stable in kimberlite magmas under upper mantle pressures and that such magmas may digest orthopyroxene sufficiently rapidly that it is very uncommon in kimberlites despite being a commonly entrained xenocryst.

Primary kimberlite melt

Experimental investigations using synthetic (e.g. Canil & Scarfe, 1990; Dalton and Presnall, 1998) and natural starting materials (e.g. Brey et al.,2008) at conditions of 4 - 12Gpa and >1300°C have aimed at replicating partial melting in the kimberlite source region. These studies have aimed at identifying the likely mineral assemblages in the source and the melting reactions by which the kimberlite melt arises. From these studies possible compositions of primary kimberlitic melts have been determined (Table1). Studies on the experimental melting of synthetic (e.g. Girnis et al. 1995; Girnis et al. 2005; Kesson et al. 1994; Ringwood et al. 1992)

and natural (e.g. Edgar and Charbonneau 1993; Edgar et al. 1988; Mitchell 2004) kimberlite have examined phase relations in the magma system at variable pressures. Other studies have focussed on geochemical analysis of natural aphanitic kimberlite to gain insight into kimberlite petrogenesis (e.g. Arndt et al. 2010; Becker and le Roex 2006; Harris et al. 2004; Kopylova et al. 2007; le Roex et al. 2003; Price et al. 2000), often estimating the composition of primary kimberlite magma (Table1). These carefully estimated compositions are however still bound to the limitations regarding our knowledge on kimberlite petrogenesis and as such assumptions regarding e.g. volatile contents and the volumes of xenocrystic olivine had to be made.

Table 1: Kimberlite melt estimations from the literature (normalized without volatiles)

	1	2	3	4	5	6 5 GPa 1320°C	6 5 GPa 1410°C	6 7 GPa 1360°C	6 7 GPa 1380°C	6 7 GPa 1450°C	7 6 GPa 1455°C	7 6 GPa 1480°C	7 6 GPa 1505°C
SiO_2	34.84	35.81	32.95	29.52	31.4 (± 3.24)	44.75	36.97	47.92	43.41	36.63	36.06	39.89	42.39
TiO_2	0.66	0.90	2.14	3.82	3.10 (± 0.84)	-	-	-	-	-	-	-	-
Al_2O_3	1.72	2.05	1.94	2.74	3.31 (± 0.54)	-	-	-	-	-	2.93	3.95	3.62
FeOT	7.01	8.39	9.35	10.89	11.57 (± 1.30)	-	-	-	-	-	-	-	-
MnO	0.18	0.20	0.22	0.22	0.23 (± 0.04)	-	-	-	-	-	-	-	-
MgO	28.89	29.39	34.86	30.82	30.26 (± 2.52)	45.14	54.91	44.08	47.98	53.45	36.66	34.94	34.60
CaO	25.00	21.21	15.92	17.71	15.92 (± 2.64)	10.12	8.12	8.00	8.61	9.92	24.36	21.22	19.40
Na_2O	0.19	0.24	0.12	0.07	0.19 (± 0.17)	-	-	-	-	-	-	-	-
K_2O	0.55	0.59	1.55	1.25	1.00 (± 0.55)	-	-	-	-	-	-	-	-
P_2O_5	0.79	0.99	0.49	2.21	2.45 (± 1.44)	-	-	-	-	-	-	-	-
SO_3	-	-	-	0.35	0.20 (± 0.18)	-	-	-	-	-	-	-	-
NiO	-	-	-	0.14	0.13 (± 0.04)	-	-	-	-	-	-	-	-
Cr_2O_3	0.17	0.23	0.44	0.26	0.22 (± 0.05)	-	-	-	-	-	-	-	-
H_2O^+ [a]	7.10	6.70	9.07	4.92	6.67 (± 2.00)								
CO_2 [a]	14.01	12.06	9.88	8.63	8.19 (± 2.90)	-	11.00	-	1.70	12.22	24.46	18.65	14.53

Sources: 1 and 2, aphanitic margin compositions JD69 and JD82 respectively from the Jericho kimberlite, Canada (Price et al. 2000); 3, calculated primitive melt for the Jericho kimberlite (Kopylova et al. 2007); 4, estimated primary melt composition for the Uintjiesberg kimberlite, South Africa (Harris et al. 2004); 5, average composition for South African close to primary group I kimberlite (Becker and le Roex 2006); 6, experimentally produced melts of synthetic peridotite + CO_2 (Canil and Belis, 1990); 7, experimentally produced kimberlitic melts in equilibtium with lherzolite (Dalton and Presnall, 1998).
[a]volatiles reported are given as in the original studies.

Experimental studies must take into account a great number of variables and, based on how these variables are dealt with, the compositions of melts produced can vary considerably. The effect of temperature variations have been proven to result in melts that range from kimberlitic to carbonatitic (Dalton and Presnall 1998) and the ratio of CO2 to H2O has been shown to strongly affect the amounts and compositions of melts produced (Girnis et al. 1995). Further variables such as pressure and starting material composition must also be considered. Despite these limitations experimental studies on the melting of mantle material provides the advantage of not having been subjected to contamination, alteration, or fractionation mentioned earlier. Upon comparing the geochemically and experimentally derived estimated primary kimberlite melt compositions one sees that the former generally have quite similar compositions and that some of the experimental compositions are quite comparable to these (e.g. the higher temperature melts of Dalton and Presnall 1998). This is however not generally the case and one typically sees that melt compositions differ considerably from one experimental study to the other (e.g. Canil and Scarfe 1990 vs Dalton and Presnall 1998), largely as a result of the variables discussed above (e.g. temperature, pressure, volatile content, starting material composition). Based on these factors and the decidedly high variability of experimentally produced melts, this work uses a natural kimberlite in its starting material that has a composition that is close-to-primary based on the work of Becker and le Roex (2006). Determining the characteristics of primary kimberlite magma, despite the difficulties associated therewith, is key to a better understanding of kimberlite petrogenesis. Even if there are still many uncertainties regarding the composition of primary kimberlite melt, there is some consensus that this magma must be very low in SiO_2, Al-poor, and rich in CO_2 (Canil and Bellis 2008; Mitchell 1995 and 2008).

Two main hypotheses for kimberlite magma generation have been proposed as a result of the studies mentioned above. The first and most widely accepted is that kimberlite magmas arise through low degrees of partial melting of metasomatized asthenospheric mantle (Becker

and le Roex 2006; Canil and Scarfe 1990; Dalton and Presnall 1998; Eggler and Wendlandt 1979; Harris et al. 2004; le Roex et al. 2003). Alternatively, higher degrees (10-20 vol%) of partial melting of metasomatized veined asthenospheric mantle has been proposed by Mitchell (1995 and 2004). Regardless of the exact method of melt generation, primary kimberlitic magmas are believed to arise through partial melting of carbonated peridotite (Wyllie and Huang 1976; Wyllie 1980).

Experimental methods

All experiments were performed using a non-end-loaded piston cylinder apparatus with a pressure plate of 10mm internal diameter. NaCl-Pyrex cells with graphite furnace tubes were employed. Temperature was monitored using type-K thermocouples and controlled with a Depths Of The Earth Temperature Control Unit (accurate to within 1°C). The error between the measured and actual temperature inside the run is estimated to be no more than ~5°C. Capsules were made from silver-palladium tubing allowing for higher temperature runs than gold, without the loss of iron associated with platinum tubing. AgPd alloys are known to be good hydrogen diffusers, and the effects thereof in this study's runs are discussed in the results section. For experiments above 1200°C Ag50Pd50 was used, lower temperature runs used Ag70Pd30. This approach limits the diffusion of hydrogen through the capsule wall at lower temperatures and prohibits capsule melting at higher temperatures.

The starting material was prepared by combining hypabyssal kimberlite (ADF1, of Becker and le Roex 2006, which is proposed to closely approximate the composition of a primary group I kimberlite magma), with mineral separates from a natural peridotite from Bultfontein (Table 2). The kimberlite sample was received in powdered form and then ground further to a homogeneous 5µm grain size under acetone. Orthopyroxene, olivine and an intergrowth of

garnet and spinel were picked from the peridotite after being crushed to ~1mm diameter. The mineral separates were then individually crushed to 115µm (±10µm). The peridotitic minerals and kimberlite were mixed in the following proportions (by weight): ADF1 88%, olivine 5%; OPX 5%; garnet-spinel intergrowth 2%. Mineral compositions are presented in Table 2. The resultant composition (Table 2) is close to that of the average primary group I kimberlite composition of Becker and le Roex (2006), with slightly higher SiO_2 and MgO owing to the addition of peridotitic material. The lower FeO and CaO concentrations, as well as higher P_2O_5 content, reflect the composition of ADF1. The H_2O content is a close match with the average, but the CO_2 is considerably lower than the average. As the estimated variation of volatile contents in natural kimberlites is substantial, the concentration of CO_2 in ADF1 is considered to be within the natural range of natural kimberlite magmas and no CO_2 was added.

The AgPd capsules were filled with ~0.03g of starting material and arc-welded shut. After testing for leaks the capsules were loaded into the furnace assembly and pressurised to 10% above the final pressure. Temperature was subsequently raised at a rate of 100°C per minute. Once the experimental temperature was reached the hot-piston out technique was employed to achieve the desired pressure. Experiments were run for 48 hours and then isobarically quenched to room temperature within 30 seconds. The capsules were then removed and checked for failure, rejecting capsules that showed any loss in mass or fractures.

Table 2: Composition of the starting material and its components.

		Kimberlite							Peridotite		
	Starting material	ADF1[a]	Ap	Phl	Spl 1[b]	Spl 2[b]	Prv	Ol	Opx	Ol	Grt-Spl intergrowth
SiO_2	29.52	26.78	-	43.09	-	-	-	42.02	58.58	41.64	47.55
TiO_2	1.54	1.75	-	1.05	11.21	6.59	57.73	-	-	-	-
Al_2O_3	2.68	2.69	-	10.29	6.45	6.30	-	-	0.87	-	13.81
Cr_2O_3	0.27	0.18	-	-	1.04	42.46	-	-	0.22	-	5.00
Nb_2O_3	-	-	-	-	-	-	0.83	-	-	-	-
Fe_2O_3	-	-	-	-	44.55	11.16	-	-	-	-	-
FeO	8.61	8.98	0.42	6.20	26.79	22.44	1.50	7.19	4.27	7.28	6.18
MnO	0.15	0.17	-	-	0.74	-	-	-	-	-	0.32
MgO	27.36	25.63	-	26.19	9.68	10.35	-	50.83	36.11	51.42	21.45
CaO	11.28	12.67	54.75	-	0.36	0.39	39.89	0.03	0.40	-	5.02
Na_2O	0.27	0.31	-	-	-	-	0.44	-	-	-	-
K_2O	0.87	0.99	-	9.76	-	-	-	-	-	-	-
P_2O_5	3.68	4.18	40.48	-	-	-	-	-	-	-	-
SO_3	0.03	0.03	-	-	-	-	-	-	-	-	-
NiO	0.15	0.16	-	-	-	-	-	0.21	-	0.27	-
F	-	-	2.67	-	-	-	-	-	-	-	-
H_2O^-	0.73	0.82	-	-	-	-	-	-	-	-	-
H_2O^+	6.95	7.89	-	-	-	-	-	-	-	-	-
CO_2	4.84	5.50	-	-	-	-	-	-	-	-	-
Total	98.92	98.73	98.32	96.57	100.81	99.68	100.39	100.28	100.44	100.61	99.33
xO^{2-} [c]			26	24	4	4	3	4	6	4	
Si			-	6.062	-	-	-	1.012	1.992	1.002	
Ti			-	0.111	0.286	0.167	0.985	-	-	-	
Al			-	1.705	0.258	0.250	-	-	0.035	-	
Cr			-	-	0.028	1.132	-	-	0.006	-	
Nb			-	-	-	-	0.009	-	-	-	
Fe^{3+}			-	-	1.142	0.283	-	-	-	-	
Fe^{2+}			0.059	0.730	0.762	0.633	0.028	0.145	0.121	0.146	
Mn			-	-	0.021	-	-	-	-	-	
Mg			-	5.492	0.49	0.520	-	1.825	1.831	1.844	
Ca			9.941	-	0.013	0.014	0.970	0.004	0.014	-	
Na			-	-	-	-	0.019	-	-	-	
K			-	1.751	-	-	-	-	-	-	
P			5.807	-	-	-	-	-	-	-	
NiO			-	-	-	-	-	0.007	-	0.005	
F			1.432	-	-	-	-	-	-	-	
∑Cations			15.81	15.85	3.00	3.00	2.01	2.99	4.00	3.00	
Mg#			-	88	39	45	-	93	94	93	

[a] Bulk Andriesfontein kimberlite composition (Becker and le Roex 2006)

[b] Two spinel populations were found in the kimberlite

[c] For apatite and phlogopite this value is ∑ (O,OH,F,Cl)

Analytical methods

Run products from successful experiments were set in epoxy with the capsule mounted lengthwise such that a vertical section through the run products was produced. Run products that were friable were impregnated with epoxy under vacuum prior to final sectioning. The samples were then polished and carbon coated. Analysis of the starting material and run products were conducted on a Zeiss EVO MA15VP SEM equipped with an Oxford X-Max EDS Silicon Drift Detector (SDD). Quantitative analysis was performed at an accelerating voltage of 20kV with a beam current of 20nA and counting time of 10s. Minerals were analyzed using a focussed beam whilst the beam was rastered over an area of 400μm^2 during analysis of the quenched melts in order to obtain a representative sample of the melts that quenched to mixtures of glass and quench crystals. Analytical accuracy was verified by analysis of standard materials of known composition and the results achieved were similar to those discussed by Diener et al. (2005). Where possible the Fe_2O_3 content of minerals was calculated in accordance with Droop (1987). A Gatan cryogenic stage fitted to the SEM was used to reduce the temperature of the sample to < -180°C when analysing the quenched melts in order to reduce migration of alkalis and hydrogen away from site of electron beam interaction during analysis. The compositions of minerals presented in this study are the average of 5 to 10 analyses, for melts they are the average of 10 to 15 analyses. The high volatile content of the starting material and the affinity for this to move into the melt as the experiments were run resulted in analysis totals for quenched melts averaging close to 80%. No systematic trends with regards to pressure and temperature were visible in this regard. Image analysis of x-ray elemental maps of the run products was used to assist the calculation of phase proportions via a least squares mixing calculation approach.

Results

The equilibrium assemblages produced in the experiments are illustrated in Fig. 1. All runs produced olivine, spinel and melt, but the presence of orthopyroxene, clinopyroxene, phlogopite and apatite varied as a function of pressure and temperature. The compositions of the phases produced are summarised in Table 3 and Table 4, additional data is given in Appendix 1 and Appendix 2.

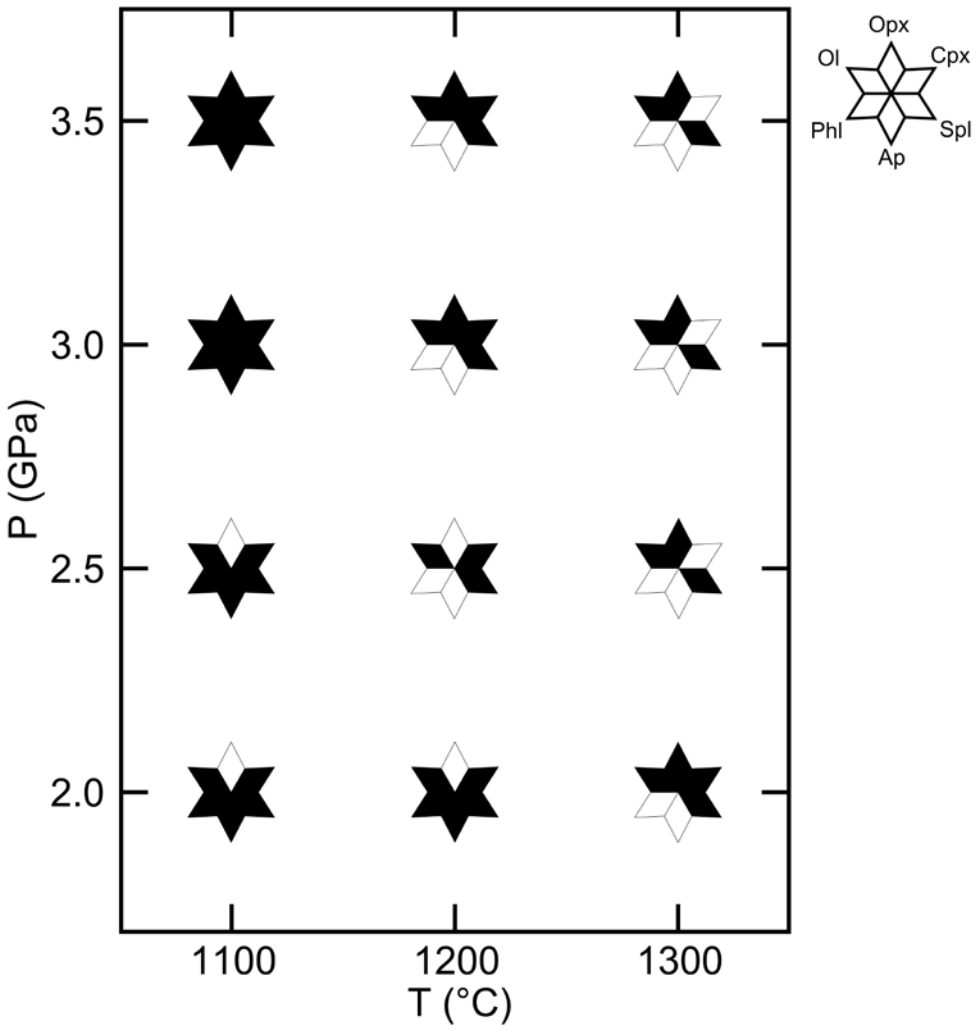

Figure 1: Run product phase assemblages shown on a P-T diagram. Filled sectors indicate the presence of the phase as indicated on the legend. All runs contain melt as an additional phase (ap = apatite; cpx = clinopyroxene; ol = olivine; opx = orthopyroxene; phl = phlogopite; spl = spinel).

Textural characteristics

As mentioned earlier, kimberlitic magmas do not quench to glass, and the experimental melts in this study all underwent quench crystallization to some degree. In all cases the melt phase could be easily identified as clearly defined melt pools, allowing for easy discrimination between quench crystals and coexisting equilibrium phases. The needle-like quench crystals were too narrow to analyze accurately and thus were not identified. Olivine crystals often exhibit euhedral shapes where they are in contact with melt indicating their equilibration with the liquid (Fig. 2a). Where they were in contact with orthopyroxene or clinopyroxene the shared boundaries were commonly rounded. Olivine crystals almost always contained inclusions of most of the other minerals present in the run products (Fig. 2b). These included grains are not believed to be relict as they do not exhibit rough, irregular borders associated with the crushed starting material. Similar to olivine, orthopyroxene also often showed a euhedral crystal habit where in contact with melt (Fig. 2d), clinopyroxene sometimes exhibited a euhedral nature, but more commonly occurred in a sub-euhedral shape. Both of the pyroxenes contain inclusions similar to those in olivine, but these are somewhat less abundant than in olivine. In some of the lower temperature runs, grains with an orthopyroxene core and clinopyroxene rim were found (Fig. 2c). These grains were most likely relict orthopyroxene seed grains, but are still assumed to be in equilibrium with the rest of the assemblages on the grounds that within these runs orthopyroxene was also found elsewhere in the mount displaying a euhedral shape and in contact with melt (Fig. 2d). Spinel was typically found as smaller grains of irregular to sub-angular shape, often as inclusions inside olivine, orthopyroxene or clinopyroxene. Apatite and phlogopite were generally of irregular shape and sometimes formed crystals as large as 200µm.

Table 3: Compositions of run product minerals.

	Ol	Ol	Ol	Ol	Ol	Ol	Ol	Ol	Ol	Ol	Ol	Ol
Exp	DK2	DK1	DK10	DK4	DK3	DK12	DK15	DK16	DK13	DK19	DK18	DK17
P (GPa)	2.0	2.0	2.0	2.5	2.5	2.5	3.0	3.0	3.0	3.5	3.5	3.5
T (°C)	1100	1200	1300	1100	1200	1300	1100	1200	1300	1100	1200	1300
SiO_2	42.03	40.80	41.32	41.16	40.92	41.35	42.44	40.95	41.51	41.22	40.96	42.38
TiO_2	-	-	-	-	-	-	-	-	-	-	-	-
Al_2O_3	-	-	-	-	-	-	-	-	-	-	-	-
Cr_2O_3	-	-	-	-	-	-	-	-	-	-	-	-
Fe_2O_3	-	-	-	-	-	-	-	-	-	-	-	-
FeO	6.86	9.84	7.99	10.13	9.67	7.37	5.49	9.23	7.74	8.61	9.21	5.71
MnO	0.04	-	-	0.05	0.06	-	-	-	-	0.02	0.03	-
MgO	51.07	48.57	50.36	48.77	48.91	50.71	52.11	49.01	50.67	49.83	49.05	51.98
CaO	0.08	0.12	0.02	-	-	-	-	-	-	-	-	-
Na_2O	-	-	-	-	-	-	-	-	-	-	-	-
K_2O	-	-	-	-	-	-	-	-	-	-	-	-
P_2O_5	-	-	-	-	-	-	-	-	-	-	-	-
NiO	0.05	0.69	0.07	0.07	0.28	0.19	0.03	0.32	0.27	0.23	0.37	0.03
F	-	-	-	-	-	-	-	-	-	-	-	-
Total	100.13	100.03	99.75	100.18	99.84	99.62	100.07	99.52	100.18	99.90	99.57	100.10
xO^{2-a}	4	4	4	4	4	4	4	4	4	4	4	4
Si	1.012	1.002	1.005	1.006	1.004	1.005	1.016	1.005	1.005	1.005	1.005	1.015
Ti	-	-	-	-	-	-	-	-	-	-	-	-
Al	-	-	-	-	-	-	-	-	-	-	-	-
Cr	-	-	-	-	-	-	-	-	-	-	-	-
Fe^{3+}	-	-	-	-	-	-	-	-	-	-	-	-
Fe^{2+}	0.138	0.202	0.162	0.207	0.198	0.150	0.110	0.189	0.157	0.175	0.189	0.114
Mn	0.001	-	-	0.001	0.001	-	-	-	-	0.000	0.001	-
Mg	1.833	1.778	1.826	1.778	1.788	1.837	1.858	1.794	1.828	1.811	1.794	1.855
Ca	0.002	0.004	0.000	-	-	-	-	-	-	-	-	-
Na	-	-	-	-	-	-	-	-	-	-	-	-
K	-	-	-	-	-	-	-	-	-	-	-	-
P	-	-	-	-	-	-	-	-	-	-	-	-
Ni	0.001	0.014	0.001	0.001	0.006	0.004	0.001	0.006	0.005	0.004	0.007	0.001
F	-	-	-	-	-	-	-	-	-	-	-	-
∑Cations	2.99	3.00	3.00	2.99	3.00	3.00	2.99	2.99	3.00	3.00	3.00	2.99
Mg#	93	90	92	90	90	92	94	90	92	91	90	94

[a]For apatite and phlogopite this value is ∑ (O,OH,F,Cl)

Table 3 continued

	Opx	Opx	Opx	Opx	Opx	Opx	Opx	Opx	Cpx	Cpx	Cpx	Cpx
Exp	DK10	DK12	DK15	DK16	DK13	DK19	DK18	DK17	DK2	DK1	DK10	DK4
P (GPa)	2.0	2.5	3.0	3.0	3.0	3.5	3.5	3.5	2.0	2.0	2.0	2.5
T (°C)	1300	1300	1100	1200	1300	1100	1200	1300	1100	1200	1300	1100
SiO_2	57.92	57.58	57.71	57.11	57.29	58.16	56.97	57.87	55.03	53.03	53.64	54.32
TiO_2	0.06	-	-	-	-	-	-	-	0.28	0.57	1.49	0.33
Al_2O_3	0.74	1.15	1.52	1.18	1.42	0.96	1.45	1.26	2.00	2.15	3.05	1.57
Cr_2O_3	0.85	0.70	0.28	0.60	0.88	0.33	0.62	0.46	0.04	0.92	1.10	0.74
Fe_2O_3	-	-	0.01	-	-	-	-	0.06	-	0.17	-	0.03
FeO	4.30	4.93	4.01	5.97	5.07	4.21	6.24	3.61	2.84	2.33	4.13	3.30
MnO	-	-	-	-	-	-	-	-	-	-	-	-
MgO	34.26	34.21	35.90	33.24	33.92	35.36	33.54	35.95	18.30	16.66	21.16	17.07
CaO	1.95	1.28	0.57	1.31	1.32	0.44	1.05	0.96	21.41	23.97	14.50	22.65
Na_2O	-	-	-	-	-	-	-	-	0.13	0.15	0.83	0.47
K_2O	-	-	-	-	-	-	-	-	-	-	-	-
P_2O_5	-	-	-	-	-	-	-	-	-	-	-	-
NiO	-	-	-	-	-	-	-	-	-	-	-	-
F	-	-	-	-	-	-	-	-	-	-	-	-
Total	100.07	99.85	99.99	99.40	99.90	99.46	99.88	100.18	100.05	99.94	99.91	100.49
$xO^{2-\ a}$	6	6	6	6	6	6	6	6	6	6	6	6
Si	1.993	1.986	1.969	1.988	1.978	2.001	1.973	1.971	1.992	1.935	1.926	1.968
Ti	0.001	-	-	-	-	-	-	-	0.008	0.016	0.040	0.009
Al	0.030	0.047	0.061	0.048	0.058	0.039	0.059	0.051	0.085	0.092	0.129	0.067
Cr	0.023	0.019	0.007	0.016	0.024	0.009	0.017	0.012	0.001	0.027	0.031	0.021
Fe^{3+}	-	-	0.000	-	-	-	-	0.002	-	0.005	-	0.001
Fe^{2+}	0.124	0.142	0.115	0.174	0.146	0.121	0.181	0.103	0.086	0.071	0.124	0.100
Mn	-	-	-	-	-	-	-	-	-	-	-	-
Mg	1.757	1.759	1.826	1.725	1.745	1.814	1.731	1.826	0.987	0.906	1.133	0.922
Ca	0.072	0.047	0.021	0.049	0.049	0.016	0.039	0.035	0.831	0.937	0.558	0.879
Na	-	-	-	-	-	-	-	-	0.009	0.011	0.058	0.033
K	-	-	-	-	-	-	-	-	-	-	-	-
P	-	-	-	-	-	-	-	-	-	-	-	-
Ni	-	-	-	-	-	-	-	-	-	-	-	-
F	-	-	-	-	-	-	-	-	-	-	-	-
∑Cations	4.00	4.00	4.00	4.00	4.00	4.00	4.00	4.00	4.00	4.00	4.00	4.00
Mg#	93	93	94	91	92	94	91	95	92	93	90	90

[a]For apatite and phlogopite this value is ∑ (O,OH,F,Cl)

Table 3 continued

	Cpx	Cpx	Cpx	Cpx	Cpx	Phl	Phl	Phl	Phl	Phl	Spl
Exp	DK3	DK15	DK16	DK19	DK18	DK2	DK1	DK4	DK15	DK19	DK2
P (GPa)	2.5	3.0	3.0	3.5	3.5	2.0	2.0	2.5	3.0	3.5	2.0
T (°C)	1200	1100	1200	1100	1200	1100	1200	1100	1100	1100	1100
SiO_2	54.25	56.97	54.81	54.00	54.41	40.20	38.96	40.42	42.55	41.05	-
TiO_2	0.21	0.03	-	0.09	-	1.09	1.79	1.63	0.61	0.68	3.62
Al_2O_3	1.27	1.33	1.07	1.48	1.34	15.10	15.07	13.80	14.56	12.95	7.20
Cr_2O_3	0.71	0.16	0.92	0.28	0.58	0.09	1.42	1.02	0.05	0.29	12.23
Fe_2O_3	0.06	-	-	-	0.03	-	-	-	-	-	48.35
FeO	2.73	2.13	3.04	3.04	3.12	3.77	3.75	4.29	2.89	4.26	18.03
MnO	-	-	-	-	-	-	-	-	-	-	-
MgO	17.37	20.69	18.45	17.79	18.04	24.21	22.63	23.01	26.00	24.08	11.52
CaO	23.48	18.81	21.23	22.30	22.32	-	-	-	-	-	-
Na_2O	0.12	0.16	0.31	0.15	0.14	0.11	0.12	0.46	0.07	0.04	-
K_2O	-	-	-	-	-	8.96	10.11	9.59	8.40	9.78	-
P_2O_5	-	-	-	-	-	-	-	-	-	-	-
NiO	-	-	-	-	-	-	0.25	-	-	-	0.58
F	-	-	-	-	-	-	-	-	-	-	-
Total	100.21	100.28	99.83	99.12	99.98	93.53	94.10	94.21	95.14	93.13	101.53
xO^{2-} [a]	6	6	6	6	6	24	24	24	24	24	4
Si	1.971	2.039	1.989	1.977	1.976	5.746	5.618	5.799	5.909	5.938	-
Ti	0.006	0.001	-	0.002	-	0.117	0.194	0.176	0.064	0.074	0.091
Al	0.054	0.056	0.046	0.064	0.057	2.544	2.561	2.333	2.383	2.207	0.283
Cr	0.020	0.004	0.026	0.008	0.017	0.011	0.162	0.116	0.005	0.033	0.322
Fe^{3+}	0.002	-	-	-	0.001	-	-	-	-	-	1.213
Fe^{2+}	0.083	0.064	0.092	0.093	0.095	0.450	0.452	0.515	0.336	0.516	0.503
Mn	-	-	-	-	-	-	-	-	-	-	-
Mg	0.941	1.104	0.998	0.971	0.977	5.159	4.864	4.922	5.382	5.192	0.573
Ca	0.914	0.721	0.826	0.875	0.869	-	-	-	-	-	-
Na	0.008	0.011	0.022	0.010	0.010	0.030	0.035	0.127	0.018	0.012	-
K	-	-	-	-	-	1.635	1.860	1.756	1.488	1.805	-
P	-	-	-	-	-	-	-	-	-	-	-
Ni	-	-	-	-	-	-	0.029	-	-	-	0.016
F	-	-	-	-	-	-	-	-	-	-	-
∑Cations	4.00	4.00	4.00	4.00	4.00	15.69	15.77	15.74	15.59	15.78	3.00
Mg#	92	95	92	91	91	92	92	91	94	91	53

[a]For apatite and phlogopite this value is ∑ (O,OH,F,Cl)

Table 3 continued

	Spl	Spl	Spl	Spl	Spl	Spl	Spl	Spl	Spl	Spl	Spl	Spl
Exp	DK2	DK1	DK10	DK4	DK4	DK3	DK12	DK12	DK15	DK15	DK16	DK13
P (GPa)	2.0	2.0	2.0	2.5	2.5	2.5	2.5	2.5	3.0	3.0	3.0	3.0
T (°C)	1100	1200	1300	1100	1100	1200	1300	1300	1100	1100	1200	1300
SiO_2	-	-	0.06	0.04	-	-	0.28	0.06	-	-	-	-
TiO_2	25.45	3.66	2.31	5.30	32.47	3.97	5.13	2.58	0.98	26.15	3.33	2.29
Al_2O_3	1.60	14.47	6.42	10.23	1.32	7.25	13.68	7.26	33.03	1.34	8.65	7.80
Cr_2O_3	4.24	45.53	52.95	35.35	6.20	40.63	42.07	41.61	32.62	6.12	44.90	42.14
Fe_2O_3	16.60	5.37	10.27	16.89	1.81	18.13	8.47	20.33	3.86	12.88	13.42	20.21
FeO	45.51	15.65	13.93	20.32	50.43	19.26	13.17	14.15	12.09	47.67	17.14	14.12
MnO	-	-	-	-	-	-	-	-	-	-	-	-
MgO	6.10	13.77	13.76	11.36	7.10	11.39	16.86	13.76	16.89	4.99	12.39	13.72
CaO	-	0.01	-	0.18	-	-	-	-	-	0.08	-	-
Na_2O	-	-	-	-	-	-	-	-	-	-	-	-
K_2O	-	-	-	-	-	-	-	-	-	-	-	-
P_2O_5	-	-	-	-	-	-	-	-	-	-	-	-
NiO	-	0.52	-	0.03	-	0.05	-	0.04	-	-	0.14	0.04
F	-	-	-	-	-	-	-	-	-	-	-	-
Total	99.49	99.00	99.70	99.75	99.31	100.69	99.65	99.78	99.48	99.24	99.96	100.32
xO^{2-} [a]	4	4	4	4	4	4	4	4	4	4	4	4
Si	-	-	0.002	0.001	-	-	0.009	0.002	-	-	-	-
Ti	0.684	0.088	0.057	0.132	0.862	0.099	0.120	0.064	0.021	0.709	0.082	0.056
Al	0.067	0.544	0.249	0.397	0.055	0.283	0.504	0.281	1.127	0.057	0.335	0.300
Cr	0.120	1.150	1.378	0.921	0.173	1.065	1.039	1.083	0.746	0.175	1.169	1.090
Fe^{3+}	0.446	0.129	0.255	0.420	0.048	0.453	0.199	0.504	0.084	0.350	0.332	0.498
Fe^{2+}	1.359	0.418	0.384	0.560	1.489	0.534	0.344	0.390	0.293	1.438	0.471	0.386
Mn	-	-	-	-	-	-	-	-	-	-	-	-
Mg	0.325	0.656	0.675	0.558	0.373	0.563	0.785	0.675	0.729	0.268	0.607	0.669
Ca	-	0.000	-	0.006	-	-	-	-	-	0.003	-	-
Na	-	-	-	-	-	-	-	-	-	-	-	-
K	-	-	-	-	-	-	-	-	-	-	-	-
P	-	-	-	-	-	-	-	-	-	-	-	-
Ni	-	0.013	-	0.001	-	0.001	-	0.001	-	-	0.004	0.001
F	-	-	-	-	-	-	-	-	-	-	-	-
∑Cations	3.00	3.00	3.00	3.00	3.00	3.00	3.00	3.00	3.00	3.00	3.00	3.00
Mg#	19	61	64	50	20	51	70	63	71	16	56	63

[a]For apatite and phlogopite this value is ∑ (O,OH,F,Cl)

Table 3 continued

	Spl	Spl	Spl	Spl	Spl	Ap	Ap	Ap	Ap	Ap
Exp	DK13	DK19	DK18	DK18	DK17	DK2	DK1	DK4	DK15	DK19
P (GPa)	3.0	3.5	3.5	3.5	3.5	2.0	2.0	2.5	3.0	3.5
T (°C)	1300	1100	1200	1200	1300	1100	1200	1100	1100	1100
SiO_2	-	-	-	-	0.20	-	-	-	-	-
TiO_2	4.73	31.54	3.19	18.88	2.99	-	-	-	-	-
Al_2O_3	15.66	1.41	7.80	1.83	13.34	-	-	-	-	-
Cr_2O_3	43.87	7.62	35.31	8.79	41.37	-	-	-	-	-
Fe_2O_3	6.10	1.56	23.83	24.04	14.96	-	-	-	-	-
FeO	12.34	51.07	18.70	41.95	8.69	0.32	0.29	0.50	0.45	0.57
MnO	-	-	-	-	-	-	-	-	-	-
MgO	17.22	5.98	11.12	4.64	18.42	0.67	0.63	0.88	0.91	1.20
CaO	-	0.25	0.01	-	-	53.26	55.36	54.51	54.22	53.27
Na_2O	-	-	-	-	-	-	-	-	-	-
K_2O	-	-	-	-	-	-	-	-	-	-
P_2O_5	-	-	-	-	-	44.11	41.96	42.19	42.05	41.65
NiO	-	-	0.12	-	-	-	-	-	-	-
F	-	-	-	-	-	1.85	1.28	1.52	1.58	1.19
Total	99.92	99.42	100.08	100.12	99.97	100.21	99.51	99.60	99.21	97.88
$xO^{2-\ a}$	4	4	4	4	4	26	26	26	26	26
Si	-	-	-	-	0.006	-	-	-	-	-
Ti	0.110	0.843	0.080	0.511	0.070	-	-	-	-	-
Al	0.569	0.059	0.307	0.078	0.487	-	-	-	-	-
Cr	1.070	0.214	0.932	0.250	1.013	-	-	-	-	-
Fe^{3+}	0.142	0.042	0.600	0.651	0.349	-	-	-	-	-
Fe^{2+}	0.318	1.517	0.523	1.262	0.225	0.046	0.040	0.070	0.062	0.080
Mn	-	-	-	-	-	-	-	-	-	-
Mg	0.791	0.317	0.554	0.249	0.851	0.171	0.154	0.218	0.228	0.302
Ca	-	0.009	0.000	-	-	9.783	9.806	9.712	9.710	9.618
Na	-	-	-	-	-	-	-	-	-	-
K	-	-	-	-	-	-	-	-	-	-
P	-	-	-	-	-	6.402	5.873	5.939	5.951	5.942
Ni	-	-	0.003	-	-	-	-	-	-	-
F	-	-	-	-	-	1.002	0.667	0.798	0.836	0.634
∑Cations	3.00	3.00	3.00	3.00	3.00	16.40	15.87	15.94	15.95	15.94
Mg#	71	17	51	16	79	-	-	-	-	-

[a]For apatite and phlogopite this value is ∑ (O,OH,F,Cl)

Table 4: Electron probe analyses of quenched melts formed in the experiments (normalized wt% anhydrous).

Exp	DK2	DK1	DK10	DK4	DK3	DK12	DK15	DK16	DK13	DK19	DK18	DK17
P (GPa)	2	2	2	2.5	2.5	2.5	3	3	3	3.5	3.5	3.5
T (°C)	1100	1200	1300	1100	1200	1300	1100	1200	1300	1100	1200	1300
SiO_2	30.62	25.94	36.96	28.79	25.94	32.45	25.53	28.3	28.55	28.75	26.81	28.28
TiO_2	1.42	3.48	2.16	3.23	3.15	2.03	2.10	2.57	2.72	1.64	3.12	2.71
Al_2O_3	8.62	5.97	4.38	6.49	4.51	5.21	6.11	5.67	4.14	7.46	4.64	3.83
Cr_2O_3	0.02	0.08	0.14	0.09	0.15	0.09	0.03	0.06	0.21	0.06	0.14	0.18
FeO	3.21	8.38	6.01	9.08	10.86	5.81	9.11	7.78	9.45	5.25	11.51	10.56
MnO	0.08	0.21	0.13	0.14	0.24	0.13	0.24	0.17	0.20	0.12	0.23	0.23
MgO	28.16	18.67	23.55	22.32	19.45	28.36	24.98	25.19	24.48	28.94	23.2	24.92
CaO	15.12	25.16	15.59	15.12	24.16	14.35	19.92	16.75	20.23	14.40	20.2	19.54
Na_2O	0.91	0.98	3.18	3.08	0.90	3.09	0.24	3.22	0.91	0.64	0.30	0.78
K_2O	0.36	2.08	1.22	1.41	0.90	1.18	0.56	1.57	1.62	1.30	0.99	1.51
P_2O_5	8.03	7.92	6.12	9.23	9.13	6.54	9.64	7.79	6.91	9.96	8.21	6.92
SO_3	0.42	0.08	0.03	0.09	0.02	0.05	0.35	0.02	0.03	0.10	0.09	0.04
NiO	0.05	0.09	0.04	0.03	0.02	0.03	0.04	0.04	0.02	0.02	0.04	0.04
F	2.97	0.95	0.51	0.90	0.57	0.67	1.14	0.88	0.52	1.36	0.53	0.47
Mg#	94	80	87	81	76	90	83	85	82	91	78	81

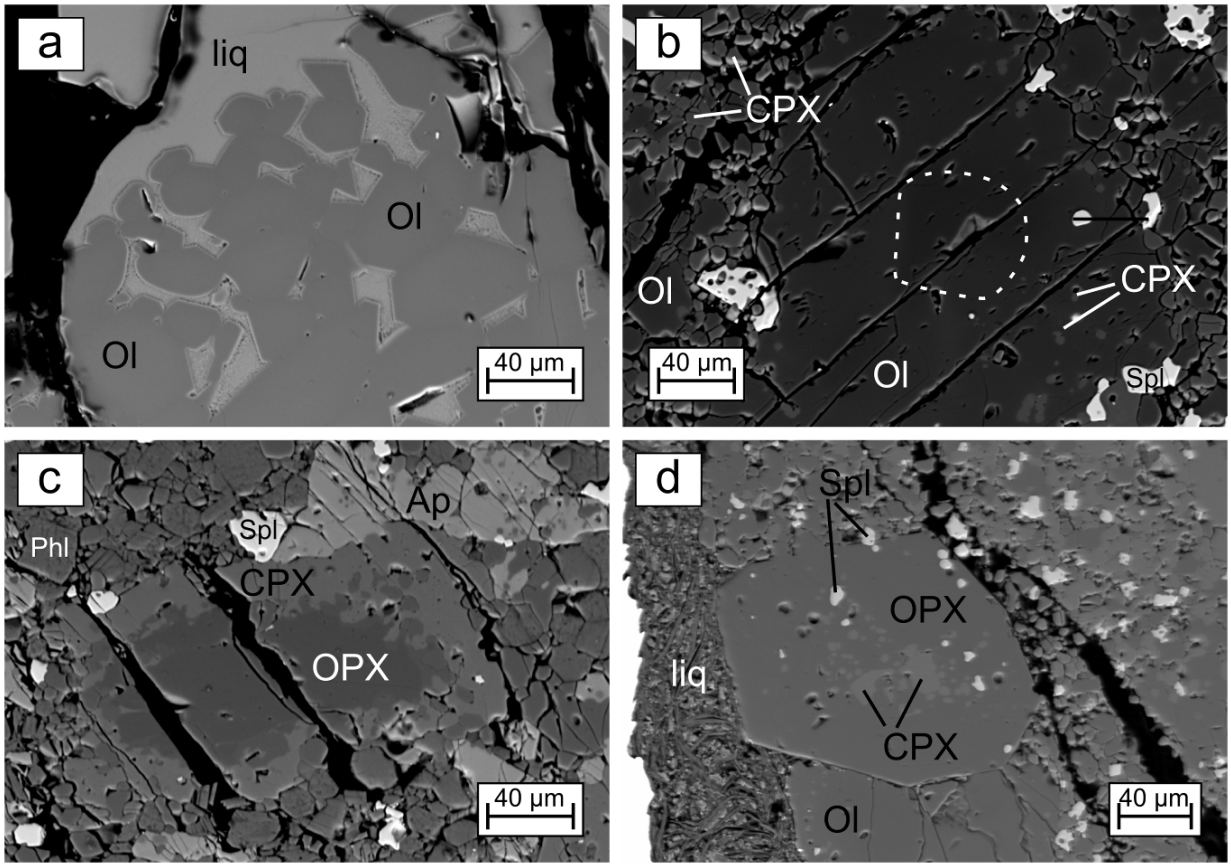

Figure 2: Back-scattered electron images showing some of the textural features in the run products. a) Euhedral olivine grains in the 1300°C, 2GPa run; b) zoned olivine with inclusions of spinel and CPX (1100°C, 3.5GPa; the dotted line encircles a core of relatively higher Mg); c) OPX in the core of a CPX grain (1100°C, 3GPa); d) Euhedral OPX grain with inclusions of CPX and spinel in the same run as c) (liq = melt). Appendix 3.1 to Appendix 3.12 provides additional images.

Phase chemistry

Olivine did not show much change in chemistry from the starting material, with Mg#'s ranging between 90 and 94 compared to the 93 in the starting material. There does not seem to be any obvious trend to the variation in Mg#'s for the runs, which is most likely controlled by phase relations. Some of the runs at 1100°C contained zoned olivine grains. These grains contained cores with Mg#'s that correspond to the starting material whereas the rims were more iron rich. Orthopyroxene compositions are very similar for all the runs (Fig. 3), with the lower temperature runs not showing much change from the peridotitic orthopyroxene in the starting

material. There is however a change to slightly more calcic orthopyroxenes with lower Mg/Fe ratios in the 1200 and 1300°C runs. The range in clinopyroxene compositions (Fig. 3) show a fair degree of variability in their Ca concentration, with the majority plotting in or close to the diopside field. The Mg#'s for orthopyroxene and clinopyroxene average at 93 and 92 respectively, with very little variation. The compositional range of spinels found in the experiments is very diverse, often with more than one species in the same run. Titanium is one of the most variable elements in the spinels ranging from close to 0% up to almost 90% ulvospinel, with a large gap between 20 and 50%. The high Ti spinels are limited to the lower temperature runs. Ignoring the high Ti spinels it is seen that the remaining spinels have chemistry ranging mostly from close to magnesiochromite (Mg# = 79) towards chromite (Mg# = 50). Among these the low temperature runs show the greatest variability whereas spinels in the 1200 and 1300°C runs group much closer together.

There is not much variation in the chemistry of the phlogopites or apatites. Worth mentioning is a trend towards slightly higher MgO and slightly lower CaO with increasing pressure in apatites and a minor loss in SiO_2 and gain in K_2O for the 1200°C phlogopite. The melts in equilibrium with the aforementioned minerals have a wide compositional range (Table 4, Fig. 4). For the most part the range in elemental concentrations can at best be described as complex, with very little obvious connections to be made with change in temperature and pressure. Al_2O_3, P_2O_5 and Cr_2O_3 show some dependency on temperature change whereby Al_2O_3 and P_2O_3 decrease in concentration with increasing temperature and Cr_2O_3 increases in concentration. In Fig. 4 the compositions of this study's melts are compared with geochemically determined estimates from the literature (Becker and le Roex 2006; Harris et al. 2004; Kopylova et al. 2007; Price et al. 2000). This study's melts are higher in Al_2O_3 and P_2O_5, increasing at lower temperatures. In the case of MgO and Cr_2O_3 the reverse is true, with this study's melts having lower concentrations that move lower still at lower temperatures. The concentration of Fe^{3+} in the FeMg silicates of all the runs is very low or zero. The spinels have higher concentrations of

Fe^{3+} but this is not uncommon for natural kimberlites (Mitchell 1986). This leads to the belief that the effect of hydrogen diffusion through the AgPd capsules could not have been significant enough to affect the outcome of the experiments in any measurable manner.

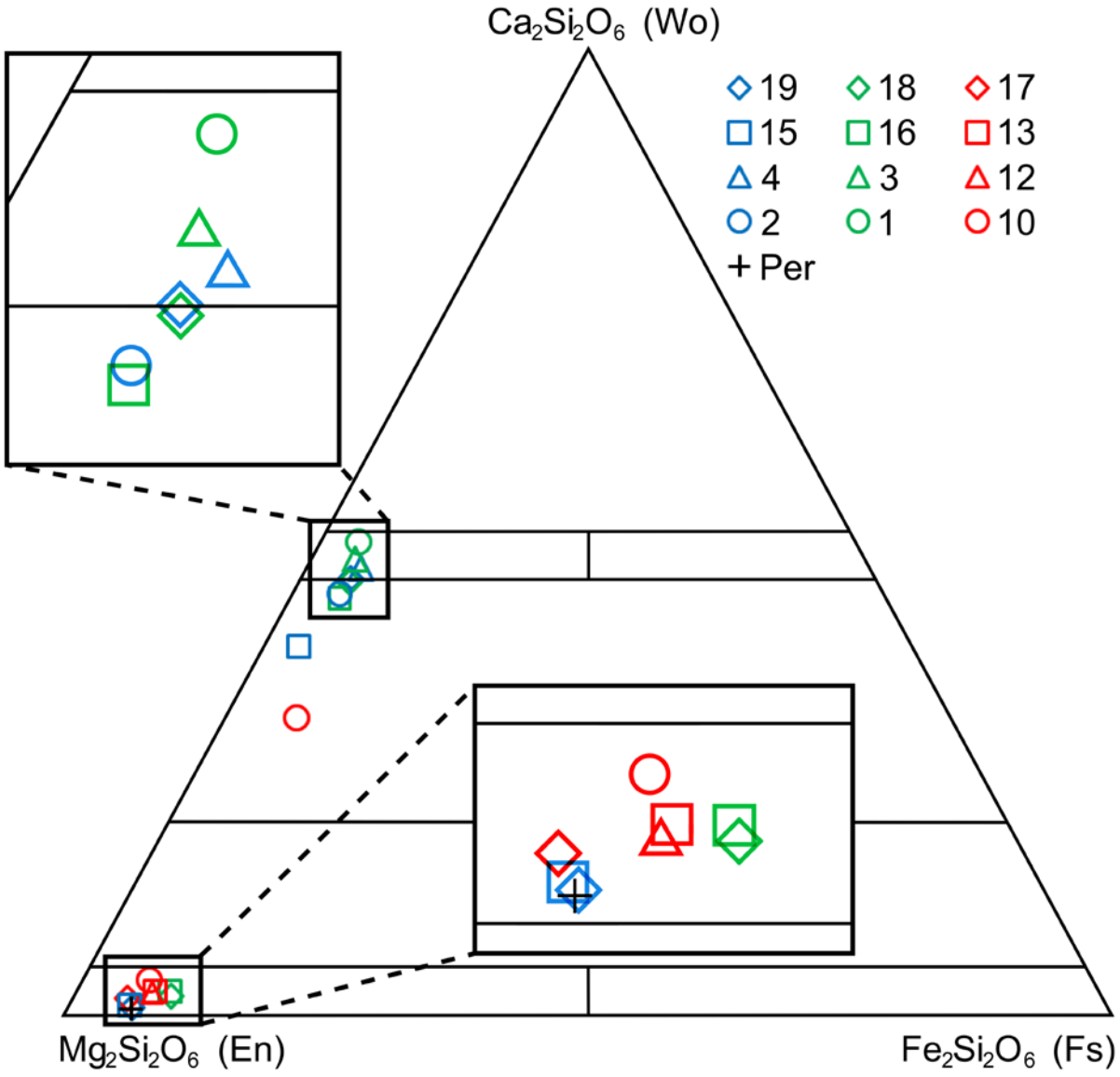

Figure 3: Compositions of pyroxenes produced in the run products. Colour corresponds to temperature (red = 1300°C; green = 1200°C; blue = 1100°C) and shapes translate to pressure (circles = 2 GPa; triangles = 2.5GPa; squares = 3 GPa; diamonds = 3.5 GPa). The composition of the OPX used in the starting material is also shown (Per) (En = enstatite; Fs = Ferrosilite; Wo = wollastonite).

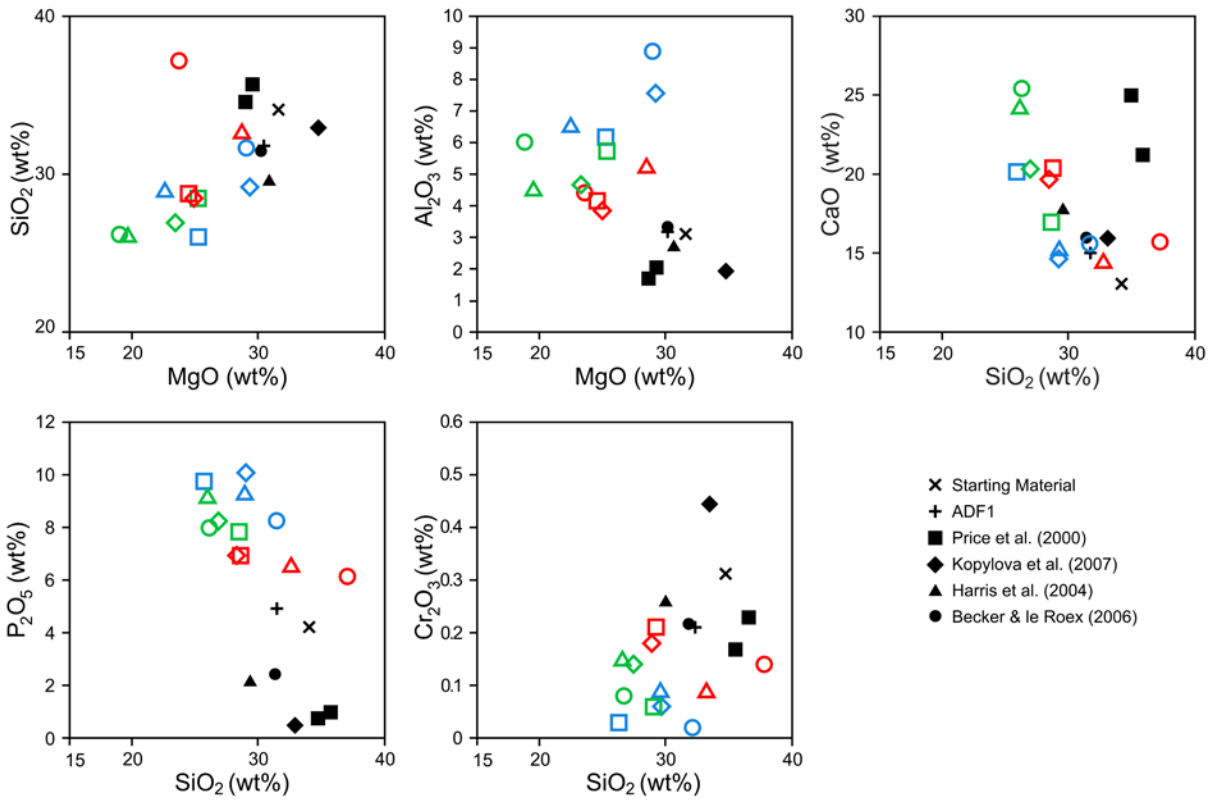

Figure 4: Compositions of melts produced in this study compared with with geochemically determined estimates of other authors. The legend for the melt compositions are the same as in Fig. 4.

Modal composition

Modal composition estimations based on mass balance calculations and image analysis were performed on all run products (see Appendix 2). The results for olivine, orthopyroxene, clinopyroxene and melt are depicted in Fig. 5 and indicate several important trends. Of the most interest is the stability of orthopyroxene at higher temperatures and pressures. In general, the amount of orthopyroxene increases with increasing temperature and pressure. To some extent olivine follows the reverse of what is seen in orthopyroxene. This is especially true for the lower pressure and temperature region where olivine reaches a maximum concentration. At somewhat higher pressures, however, olivine shows a somewhat consistent concentration, apparently less affected by temperature change. Clinopyroxene is stable over the largest part of

the experimental range, only being absent in the 2.5, 3.0 and 3.5 GPa runs at 1300°C. It shows fairly straightforward temperature dependence, with amounts increasing towards lower temperatures. The proportion of melt in the runs increases with temperature, seemingly independent of pressure change. Not shown in Fig. 5 are the modal compositions for phlogopite, apatite and spinel (refer to Appendix 2). Apatite and phlogopite are both stable phases in the lower temperature runs, but differ in abundance in relation to pressure, with the former being more abundant at lower pressure and the latter at higher pressures. There are no clear relationships between spinel abundance and temperature or pressure.

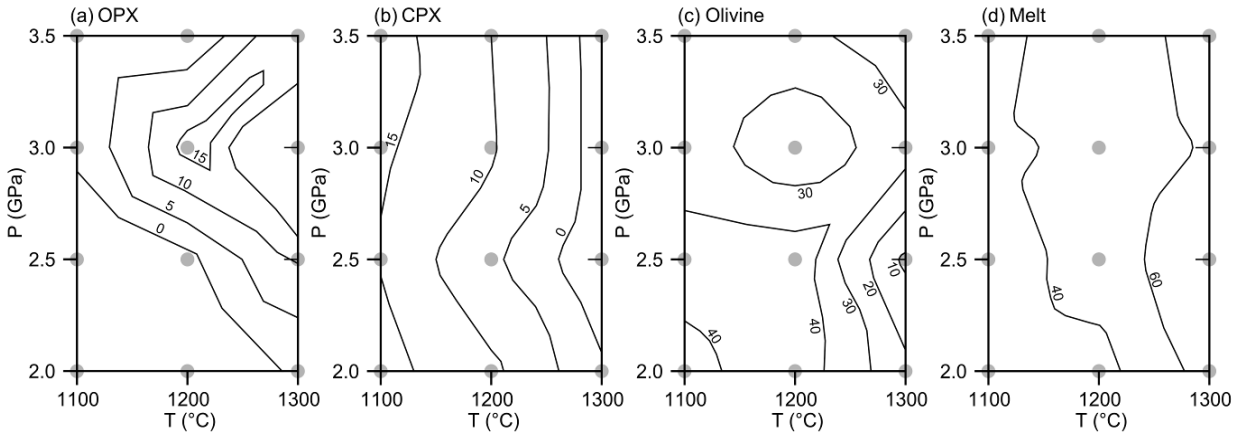

Figure 5: Modal phase contours for a) OPX, b) CPX, c) olivine and d) melt. Data points used are shown as grey dots. Contours represent percentage of the total wt% of the runs and are marked on the side of increasing concentration.

Discussion

The pressures at which these experiments were conducted equates roughly to a depth range of 70-115 km. This study therefore does not simulate the PT conditions at the 150-200 km depth where diamond bearing kimberlite magma is widely believed to originate. What this study

does provide is a window into mineral stability within kimberlite magma as it ascends through the upper mantle. The range in experimental temperatures also corresponds well with the low degree of magma cooling associated with the rapid ascent of kimberlitic magma. The temperature at the source of kimberlite melt is estimated at 1200-1400°C (Dalton and Presnall 1998; Priestley et al. 2006), which is expected to fall to ~1150°C by the time it reaches a pressure of ~2 GPa (Wilson and Head 2007). In light of the aforementioned, the melts produced in the runs of this study cannot be taken to represent primary kimberlite melt compositions, as these runs were not designed to investigate ascent from the origin. The compositions of these melts are therefore better described as snapshots of the evolution of a primary kimberlitic melt as it ascends trough the upper mantle.

A general trend is seen in the major elements whereby the composition of the melts evolve up temperature towards close-to-primary kimberlite compositions and the experimental melt compositions of Dalton and Presnall (1998). Considering that this study's melt compositions are snapshots of kimberlitic melt evolution through P-T space rather than primary melt compositions affords us the ability to infer that if we were to subject the runs to higher temperatures and pressures approaching conditions at the source, according to the aforementioned trend, similar compositions as produced by most authors shown in Fig 4 (due to fairly large compositional differences, Kopylova et al. 2007 are excluded here) would be reached. This brings credibility to these authors prediction of kimberlite petrogenesis and leads this study, based on the starting material used, to believe their conclusions that primary kimberlite melt could form by low degrees (0.5-1%) of partial melting of carbonated garnet lherzolite.

The occurrence of phlogopite in the lower pressure runs, but not at higher pressures suggests that it is not as stable at depth as it is at shallower levels of eruption. It's presence in the low pressure 1200°C run seems to imply that lower pressure is beneficial to phlogopite

stability. Volatile abundance is likely to play a vital role in phlogopite stability as well. Had there been more water available the runs could have produced more melt, potentially removing phlogopite from the assemblage altogether.

Orthopyroxene and olivine in kimberlitic melts

The solubility of orthopyroxene in this study's kimberlitic melts is highly dependent on the pressure and temperature conditions that the run is subjected to (Fig. 5a). At lower temperatures and pressures it is found that the orthopyroxene is so unstable that even in the natural kimberlite sample used in this study 5 wt% thereof is easily reacted out. This removal of orthopyroxene could result from either congruent or incongruent dissolution into the melt. The former requires that the composition of the melt formed become depleted in Ca relative to the bulk (Fig. 6 reaction A), whereas the latter allows for melt compositions of similar Ca, but higher Si than the bulk. The compositions of the melts produced in this study, including these lower temperature and pressure runs, all plot in a relatively Ca and Si enriched area, a scenario better explained by incongruent melting with olivine as a peritectic product (Fig. 6 reaction B). This would inhibit the movement of melt composition away from Ca, as would be the case if reaction A (Fig. 6) was in effect. The increased concentrations of olivine in this region whereby olivine modal phase contours are more or less the inverse of orthopyroxene (Fig. 5a and c) also suggests that olivine forms as orthopyroxene dissolves consistent with an incongruent melting model.

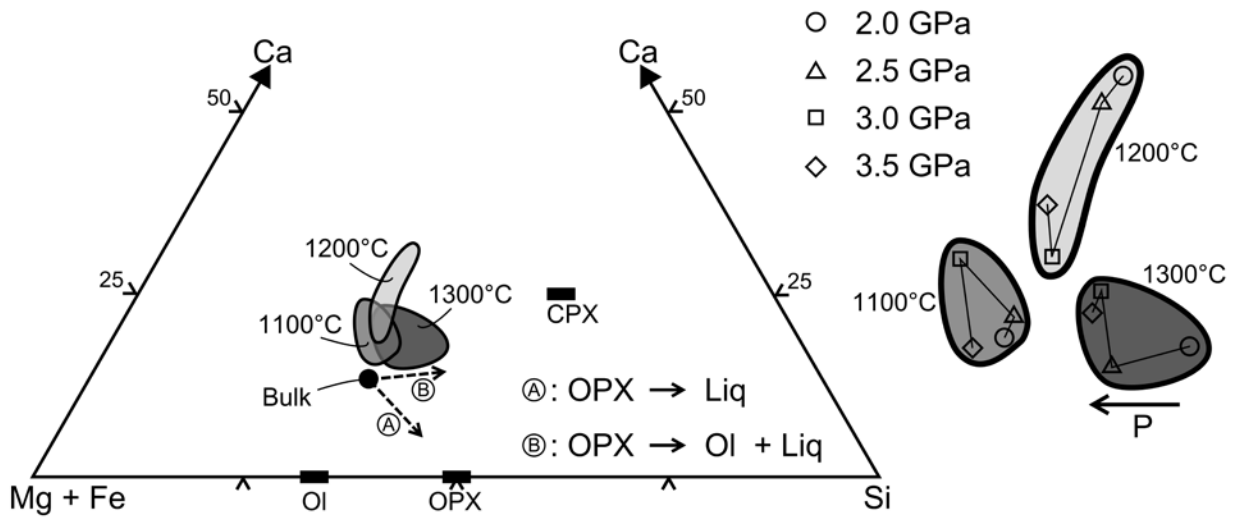

Figure 6: Compositions of melts produced in this study plotted in terms of their molar Ca, Mg, Fe, and Si, and compared to the compositions of the starting material. The compositions are shown as areas shaded according to temperature on the ternary diagram, these areas are separated and the individual compositions shown to the right. Also shown on the ternary diagram is A) the effect of complete orthopyroxene dissolution on the melt composition and B) the effect on the melt composition if orthopyroxene melting is incongruent. For reference, the positions of olivine, orthopyroxene and clinopyroxene are shown. Bulk is equivalent to the composition of the starting material. Molar compositions for melts are given in Appendix 1.

At higher temperature and pressure conditions orthopyroxene stability increases such that in many runs the volume thereof is higher than in the starting material (Fig. 5a). This implies that the kimberlite used in the starting material, which was devoid of orthopyroxene, must have dissolved its entire orthopyroxene population prior to emplacement and probably before it ascended to a depth equivalent to 2.5GPa (~85km). The inverse stability of olivine is not as convincing at the higher temperatures and pressures, probably controlled by more complex reactions, however evidence for incongruent reaction between olivine and orthopyroxene can be seen in their textural relationships. The lack of straight grain boundaries between the two as well as the observation that these minerals are commonly found as inclusions in each other (Fig. 7) is interpreted as proof of simultaneous crystallization and incongruent reaction. Kamenetsky et al. (2009) studied the inclusions of orthopyroxene in groundmass olivine and concluded that they are most likely relics of orthopyroxene from deep origin that was assimilated by the ascending kimberlite magma. In this study, the increasing stability of orthopyroxene towards

higher temperature and pressure also favours this method for the production of orthopyroxene inclusions in natural kimberlite.

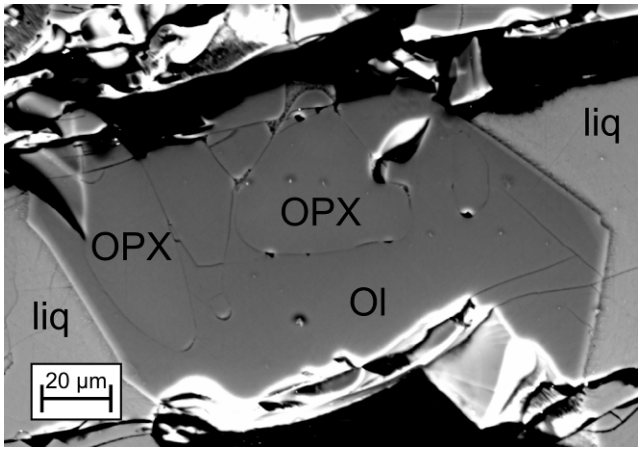

Figure 7: Back-scattered electron image of rounded orthopyroxene inclusions inside a euhedral olivine grain.

Some of the runs produced relatively large volumes of orthopyroxene, often higher than what was originally introduced into the starting material. This, along with the assumption that at lower temperatures and pressures it melts incongruently to form olivine, implies that a fairly large percentage of this olivine originates as the peritectic product of this reaction. If we subtract the orthopyroxene that was introduced to the starting material from the total volume of orthopyroxene in the runs, we find that a maximum of ~10 wt% orthopyroxene is added to the assemblage by equilibration. This orthopyroxene must have formed from the original kimberlite used in the starting material. To the ascending magma this means that ~7.5 wt% olivine is added between the depths equivalent to roughly 3.5 and 2.5 GPa (115 and 85 km respectively). This equates to ~8 vol% orthopyroxene melting to form ~5.5 vol% olivine. This value is much lower than the 25 vol% olivine traditionally thought to be phenocrysts in kimberlite (e.g. Mitchell 2008), but slightly higher than the 5 vol% of Brett et al. (2009). One must also consider that this study has only covered a section of kimberlite ascent through the sub-continental lithospheric mantle, and that it is likely that at higher pressures orthopyroxene volumes might be higher still,

resulting in higher than 5.5 vol% olivine crystallization at lower pressures. It is however unlikely that the volume of olivine that formed during the ascent of the magma could be as high as 25 vol%.

Fig. 6 compares this study's melts as a function of Ca, Mg, Fe and Si, and what is immediately evident is that temperature plays an important role in their composition, allowing to group the different temperature runs. The 1100°C melt compositions plot the furthest from the starting material composition and appear to be largely controlled by olivine crystallization. These runs have relatively high volumes of olivine (Fig. 5c) in their assemblage averaging at 38 modal %. The melts produced in the 1200°C experiments also appear to be controlled by olivine, with a similar but slightly lower average modal olivine of 36%, however, these melts plot much closer to the starting material composition. This could be a result of the higher melt volume produced in the 1200°C runs (Fig. 5d), decreasing the effect of olivine precipitation on the Ca concentration of the melt. In the 1300°C melts a decreased effect of olivine crystallization and a shift towards higher Si is seen. This shift can be explained by the absence or low volume of clinopyroxene in these runs (Fig. 5b). The shift in composition marks a lower dependence on olivine precipitation, and is reflected in the average modal olivine of 21%. Figure 6 shows that the 1200°C melts are considerably more Ca rich than the 1100 and 1300°C melts. This result is thought to be related to the breakdown of apatite just below 1200°C. As apatite is dissolved into the melt, it becomes enriched in Ca relative to the 1100°C runs. As temperature is increased further to 1300°C more melt is produced and the Ca content is diluted.

Within each temperature group there is a vague but undeniable trend by which an increase in pressure lowers the Si content of the melt (Fig. 6). At first glance this is not in agreement with the notion that orthopyroxene is unstable in low SiO_2 activity melts (Luth 2009; Mitchell 1973; Mitchell 2008). As mentioned earlier, SiO_2 activity in a fluid coexisting with olivine and

orthopyroxene is expected to decrease with decreasing pressure, thus allowing for the incongruent dissolution of orthopyroxene. This pressure controlled orthopyroxene dissolution is precisely what is seen in the runs (Fig. 5a), leading to the belief that this study's orthopyroxene dissolution is indeed in agreement with previous studies and that the weak pressure trend visible in Fig. 6 is most likely coincidental and controlled by the complex nature of our run product assemblages.

Conclusion

Through simulating the pressure and temperature conditions of the sub-continental lithospheric mantle that kimberlite magmas are thought to ascend through, this study has investigated the stability of orthopyroxene in these magmas.

This study's experiments found that at pressures higher than 2.5 GPa orthopyroxene can be a stable phase in equilibrium with a kimberlitic magma, but that at lower pressures it melts incongruently to form olivine and enriches the melt in SiO_2. This peritectic olivine population is interpreted to contribute a maximum of 5.5 vol% to the kimberlite assemblage for the pressures and temperatures examined here. This addresses both the problems of determining the volumes of phenocrystic olivine in natural kimberlites as well as the manner in which orthopyroxene is removed from the xenocrystic assemblage entrained by the kimberlite upon ascent.

Furthermore, although the melts produced in this study cannot be considered as primary melt estimates, they still agree well with the compositions of primary melts from the literature. It is found that in this study's experiments, the compositions of the melts produced rely heavily on the exact pressures and temperatures the runs were subjected to. This suggests that in order to determine the true primary compositions of naturally occurring kimberlites one needs to carefully

consider the ascent of the kimberlite in question through pressure and temperature space. Considering this in future studies could lead to more accurate estimations of primary kimberlite melt compositions and help clarify chemical differences between various kimberlites.

References

Arndt NT, Guitreau M, Boullier AM, le Roex A, Tommasi A, Cordier P, Sobolev A (2010) Olivine , and the Origin of Kimberlite. J Petrol 51:573-602

Becker M, le Roex AP (2006) Geochemistry of South African On- and Off-craton, Group I and Group II Kimberlites: Petrogenesis and Source Region Evolution. J Petrol 47:673-703

Brett RC, Russell JK, Moss S (2009) Origin of olivine in kimberlite: Phenocryst or impostor?. Lithos 112S:201-212

Brey GP, Bulatov VK, Girnis AV, Lahaye Y (2008) Experimental Melting of Carbonated Peridotite at 6-10GPa. J Petrol 49:797-821

Canil D, Bellis AJ (2008) Phase equilibria in a volatile-free kimberlite at 0.1 Mpa and the search for primary kimberlite magma. Lithos 105:111-117

Canil D, Scarfe CM (1990) Phase Relations in Peridotite + CO2 Systems to 12 GPa: Implications for the Origin of Kimberlite and Carbonate Stability in the Earth's Upper Mantle. J Geophys Res 95:15805-15816

Clement CR (1982) A comparative geological study of some major kimberlite pipes in the Northern Cape and Orange Free State. PhD thesis, Univ Cape Town, South Africa

Dalton JA, Presnall DC (1998) The Continuum of Primary Carbonatitic–Kimberlitic Melt Compositions in Equilibrium with Lherzolite: Data from the System CaO–MgO–Al2O3–SiO2–CO2 at 6 GPa. J Petrol 39:1953-1964

Dawson JB (1980) Kimberlites and their xenoliths. Springer-Verlag, Berlin

Diener JFA, Stevens G, Kisters AFM, Poujol M (2005) Metamorphism and exhumation of the basal parts of the Barberton greenstone belt, South Africa: Constraining the rates of Mesoarchaean tectonism. Precambrian Res 143:87-112

Droop, G.T.R., 1987. A general equation for estimating Fe^{3+} concentrations in ferromagnesian silicates and oxides from microprobe analyses using stoichiometric criteria. Mineral Mag 51:431-435.

Edgar AD, Arima M, Baldwin DK, Bell DR, Shee SR, Skinner EMW, Walker EC (1988) High pressure high temperature melting experiments on a SiO2-poor aphanitic kimberlite from the Wesselton mine, Kimberley, South Africa. Am Mineral 73:524-533

Edgar AD, Charbonneau HE (1993) Melting experiments on a SiO2-poor, CaO rich aphanitic kimberlite from 5-10 GPa and their bearing on sources of kimberlite magmas. Am Mineral 78:132-142

Eggler DH (1973) Role of CO2 in melting processes in the mantle. Carnegie Inst Washington Yearbook 72: 457-467

Eggler DH, Wendlandt RF (1979) Experimental studies on the relationship between kimberlite magmas and partial melting of peridotite. In: Boyd FR, Meyer HOA (eds) Kimberlites, diatremes, and diamonds: their geology petrology and geochemistry. American Geophysical Union, Washington, pp 330–338

Girnis AV, Brey GP, Ryabchikov ID (1995) Origin of Group IA Kimberlites: Fluid-saturated melting experiments at 45 – 55 kbar. Earth Planet Sci Lett 134:283-296

Girnis AV, Bulatov VK, Brey GP (2005) Transition from Kimberlite to Carbonatite Melt under Mantle Parameters: An Experimental Study. Petrology 13:1-15

Gudfinnsson GH, Presnall DC (2005) Continuous Gradations among Primary Carbonatitic, Kimberlitic, Melilititic, Basaltic, Picritic, and Komatiitic Melts in Equilibrium with Garnet Lherzolite at 3–8 GPa. J Petrol 46:1645-1659

Harris M, le Roex AP, Class C (2004) Geochemistry of the Uintjiesberg kimberlite, South Africa: petrogenesis of an off-craton, group I kimberlite. Lithos 74:149-165

Kamenetsky MB, Sobolev AV, Kamenetsky VS, Maas R, Danyushevsky RT, Pokhilenko NP, Sobolev NV (2004) Kimberlite melts rich in alkali chlorides and carbonates: A potent metasomatic agent in the mantle. Geology 32:845-848

Kamenetsky VS, Kamenetsky MB, Sharygin VV, Faure K, Golovin AV (2007) Chloride and carbonate immiscible liquids at the closure of the kimberlite magma evolution (Udachnaya-East kimberlite, Siberia). Chem Geol 237:384-400

Kamenetsky VS, Kamenetsky MB, Sobolev AV, Golovin AV, Sharygin VV, Pokhilenko NP, Sobolev NV (2009) Can pyroxenes be liquidus minerals in the kimberlite magma?. Lithos 112:213-222

Keshav S, Corgne A, Gudfinnsson GH, Bizimis M, McDonough WF, Fei Y (2005) Kimberlite petrogenesis: Insights from clinopyroxene-melt partitioning experiments at 6 GPa in the CaO-MgO-Al2O3-SiO2-CO2 system. Geochim Cosmochim Acta 69:2829-2845

Kesson SE, Ringwood AE, Hibberson WO (1994) Kimberlite melting relations revisited. Earth Planet Sci Lett 121:261-262

Kopylova MG, Matveev S, Raudsepp M (2007) Searching for parental kimberlite melt. Geochim Cosmochim Acta 71:3616-3629

Le Roex AP, Bell DR, Davis P (2003) Petrogenesis of group I kimberlites from Kimberley, South Africa: evidence from bulk rock geochemistry. J Petrol 44:2261-2286

Luth RW (2009) The activity of silica in kimberlites, revisited. Contrib Mineral Petrol 158:283-294

McDonald I, Viljoen KS (2006) Platinum-group element geochemistry of mantle eclogites: a reconnaissance study of xenoliths from the Orapa kimberlite, Botswana. Appl Earth Science (Trans Inst Min Metall B) 115:81-93

Mitchell RH (1973) Composition of olivine, silica activity and oxygen fugacity in kimberlite. Lithos 6:65-81

Mitchell RH (1986) Kimberlites: Mineralogy, Geochemistry and Petrology. Plenum Press, New York

Mitchell RH (1995) Kimberlites, Orangeites, and Related Rocks. Plenum Press, New York

Mitchell RH (2004) Experimental studies At 5–12 GPa of the Ondermatjie hypabyssal kimberlite. Lithos 76:551-564

Mitchell RH (2008) Petrology of hypabyssal kimberlites: Relevance to primary magma compositions. J volcanol Geotherm Res 174:1-8

Price SE, Russell JK, Kopylova MG (2000) Primitive magma from the Jericho Pipe N.W.T., Canada: Constraints on primary kimberlite melt chemistry. J Petrol 41:789-808

Priestley K, McKenzie D, Debayle E (2006) The state of the upper mantle beneath southern Africa. Tectonophys 416:101-112

Ringwood AE, Kesson SE, Hibberson W, Ware N (1992) Origin of kimberlites and related magmas. Earth Planet Sci Lett 113:521-538

Ryabchikov ID, Girnis AV (2005) Genesis of low calcium kimberlite magmas. Russian Geol Geophysics 46:1223-1233

Sparks RSJ, Baker L, Brown RJ, Field M, Schumacher J, Stripp G, Walters A (2006) Dynamical constraints on kimberlite volcanism. J volcanol Geotherm Res 155:18-48

Wilson L, Head JW (2007) An integrated model of kimberlite ascent and eruption. Nature 447:53-57

Wyllie PJ, Huang WL (1976) Carbonation and Melting Reactions in the System CaO–MgO–SiO2–CO2 at Mantle Pressures with Geophysical and Petrological Applications. Contrib Mineral Petrol 54:79-107

Wyllie PJ (1980) The Origin of Kimberlite. J Geophys Res 85:6209-6910

Appendices

Appendix 1: Electron probe analyses of quenched melts formed in the experiments (recalculated to molar concentration).

Exp	DK2	DK1	DK10	DK4	DK3	DK12	DK15	DK16	DK13	DK19	DK18	DK17
P (GPa)	2	2	2	2.5	2.5	2.5	3	3	3	3.5	3.5	3.5
T (°C)	1100	1200	1300	1100	1200	1300	1100	1200	1300	1100	1200	1300
Si	10.93	9.94	13.47	10.68	9.97	11.77	9.55	10.48	10.78	10.39	10.21	10.71
Ti	0.38	1	0.59	0.9	0.91	0.55	0.59	0.72	0.77	0.45	0.89	0.77
Al	3.63	2.69	1.88	2.84	2.04	2.23	2.7	2.48	1.84	3.18	2.08	1.71
Cr	0.01	0.02	0.04	0.03	0.05	0.03	0.01	0.02	0.06	0.02	0.04	0.05
Fe	0.96	2.68	1.83	2.82	3.49	1.76	2.85	2.41	2.98	1.59	3.67	3.34
Mn	0.03	0.07	0.04	0.04	0.08	0.04	0.08	0.05	0.06	0.04	0.07	0.07
Mg	14.98	10.66	12.8	12.34	11.14	15.34	13.93	13.9	13.77	15.59	13.17	14.07
Ca	5.78	10.33	6.09	6.01	9.95	5.58	7.99	6.64	8.18	5.58	8.24	7.93
Na	0.63	0.73	2.25	2.21	0.67	2.17	0.17	2.31	0.67	0.45	0.22	0.57
K	0.16	1.02	0.57	0.67	0.44	0.55	0.27	0.74	0.78	0.6	0.48	0.73
P	2.42	2.57	1.89	2.9	2.97	2.01	3.05	2.44	2.21	3.05	2.65	2.22
S	0.11	0.02	0.01	0.02	0.01	0.01	0.1	0	0.01	0.03	0.02	0.01
Ni	0.01	0.03	0.01	0.01	0.01	0.01	0.01	0.01	0.01	0.01	0.01	0.01
F	3.35	1.15	0.58	1.06	0.69	0.77	1.35	1.03	0.62	1.55	0.64	0.57
O	56.62	57.08	57.94	57.46	57.57	57.18	57.35	56.78	57.25	57.49	57.6	57.25

Appendix 2: Modal composition estimates for run products. Modal compositions for run products were calculated by combining the results of mass balance calculations with image analysis of the run products. Mass balance was done by linear least squares regression using the data presented in tables 2, 3 and 4. Image analysis was done by x-ray elemental mapping of the run products. These elemental maps were then used to identify and outline the various phases within each run. From this the areas associated with each phase could be determined. The final modal composition of each run was determined by first performing linear least squares regression. This was compared to the results of the image analysis and in cases where the linear least squares regression failed to assign appropriate proportions to phases a maximum or minimum percentage was assigned. In assigning these limits the relatively large density difference between some of the phases (e.g. olivine and melt) was taken into account and the limits were weighted accordingly.

Exp	DK2	DK1	DK10	DK4	DK3	DK12	DK15	DK16	DK13	DK19	DK18	DK17
P (GPa)	2	2	2	2.5	2.5	2.5	3	3	3	3.5	3.5	3.5
T (°C)	1100	1200	1300	1100	1200	1300	1100	1200	1300	1100	1200	1300
Opx	0.0	0.0	0.4	0.0	0.0	10.0	0.8	15.0	0.6	0.1	0.6	11.7
Cpx	16.7	11.0	0.0	14.5	5.6	0.0	15.9	10.5	0.0	17.4	10.0	0.0
Ol	36.2	46.4	22.5	43.7	43.5	8.2	35.0	20.9	35.0	36.2	35.0	20.0
Spl	8.9	5.4	9.2	5.1	1.2	7.1	7.5	8.6	1.6	6.9	1.1	3.6
Phl	0.2	0.3	0.0	0.4	0.0	0.0	1.0	0.0	0.0	0.9	0.0	0.0
Ap	6.6	3.5	0.0	7.3	0.0	0.0	4.0	0.0	0.0	5.7	0.0	0.0
Melt	31.3	33.4	67.8	29.1	49.7	74.7	35.8	45.0	62.8	32.8	53.3	64.6

Appendix 3.1: Back-scattered electron images of experiment DK2 (2.0 GPa, 1100°C).

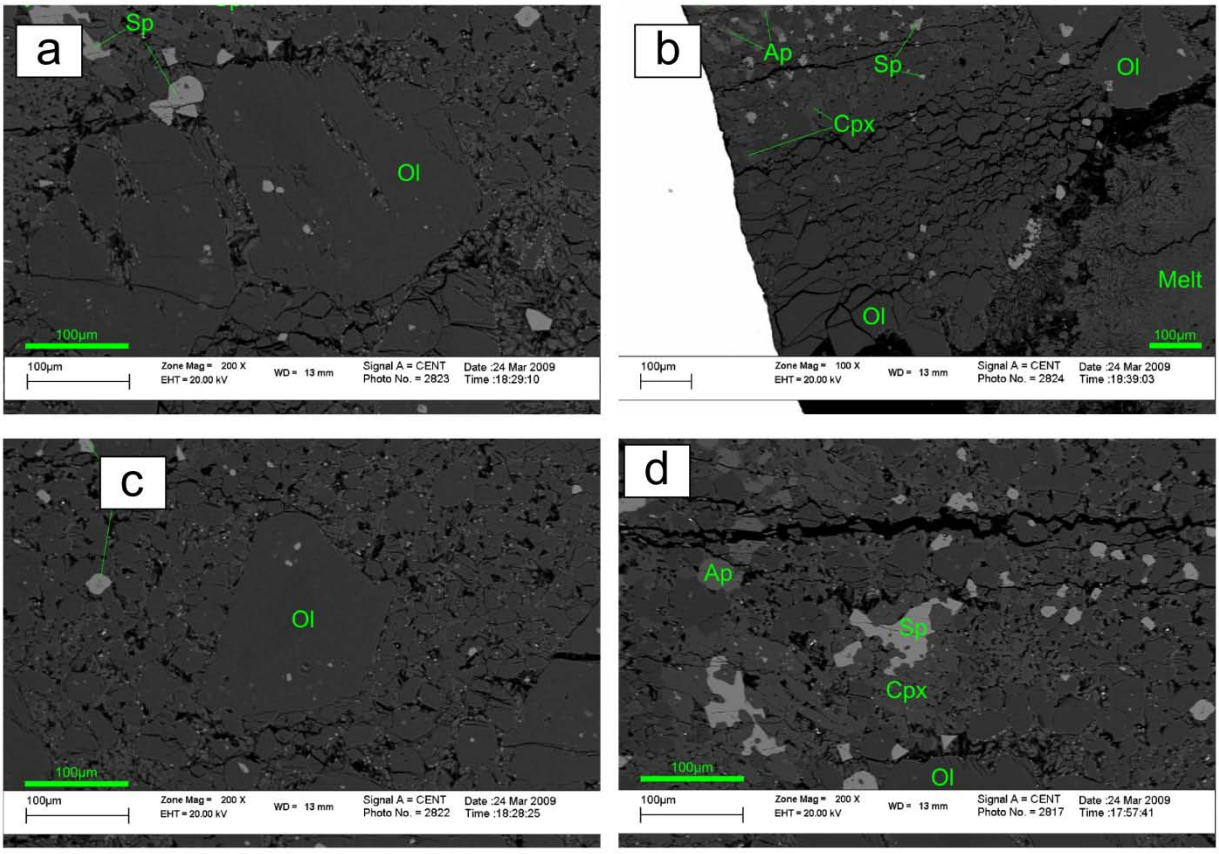

Appendix 3.2: Back-scattered electron images of experiment DK1 (2.0 GPa, 1200°C).

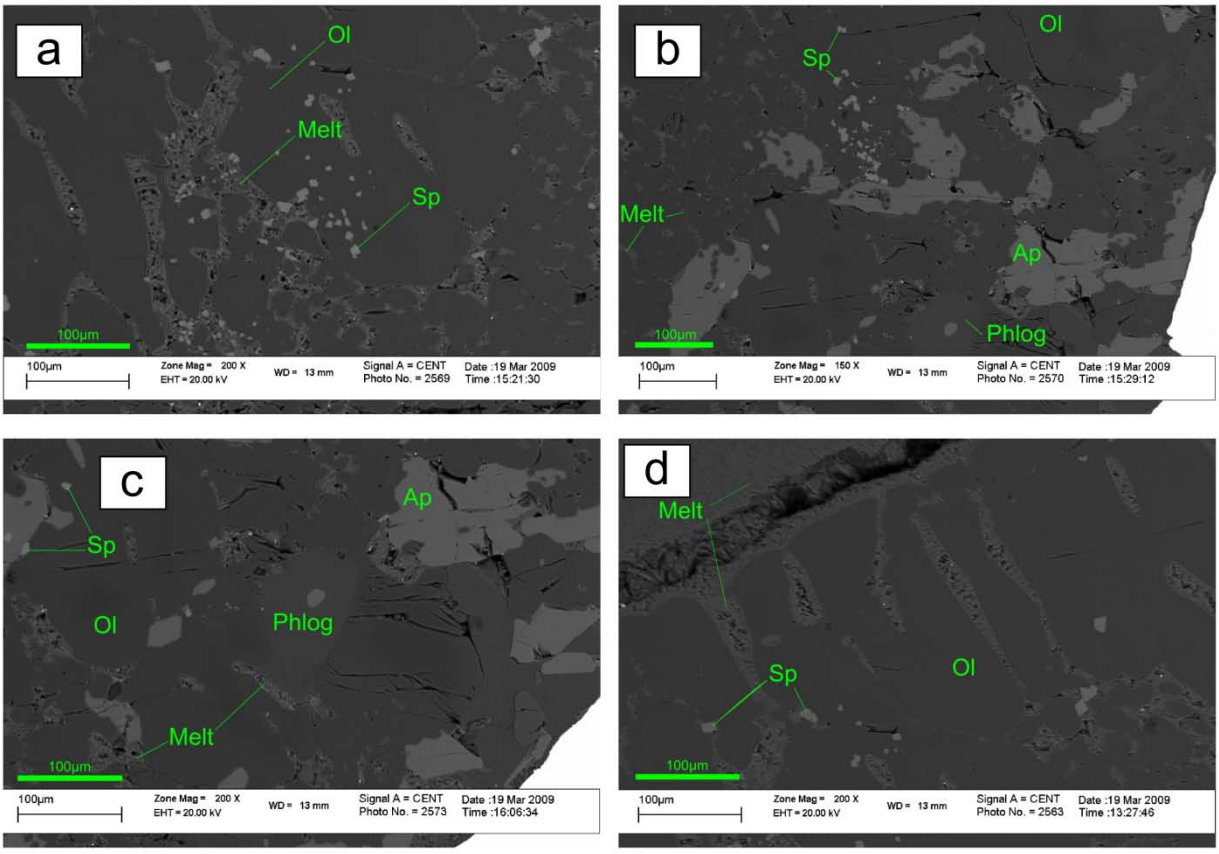

Appendix 3.3: Back-scattered electron images of experiment DK10 (2.0 GPa, 1300°C).

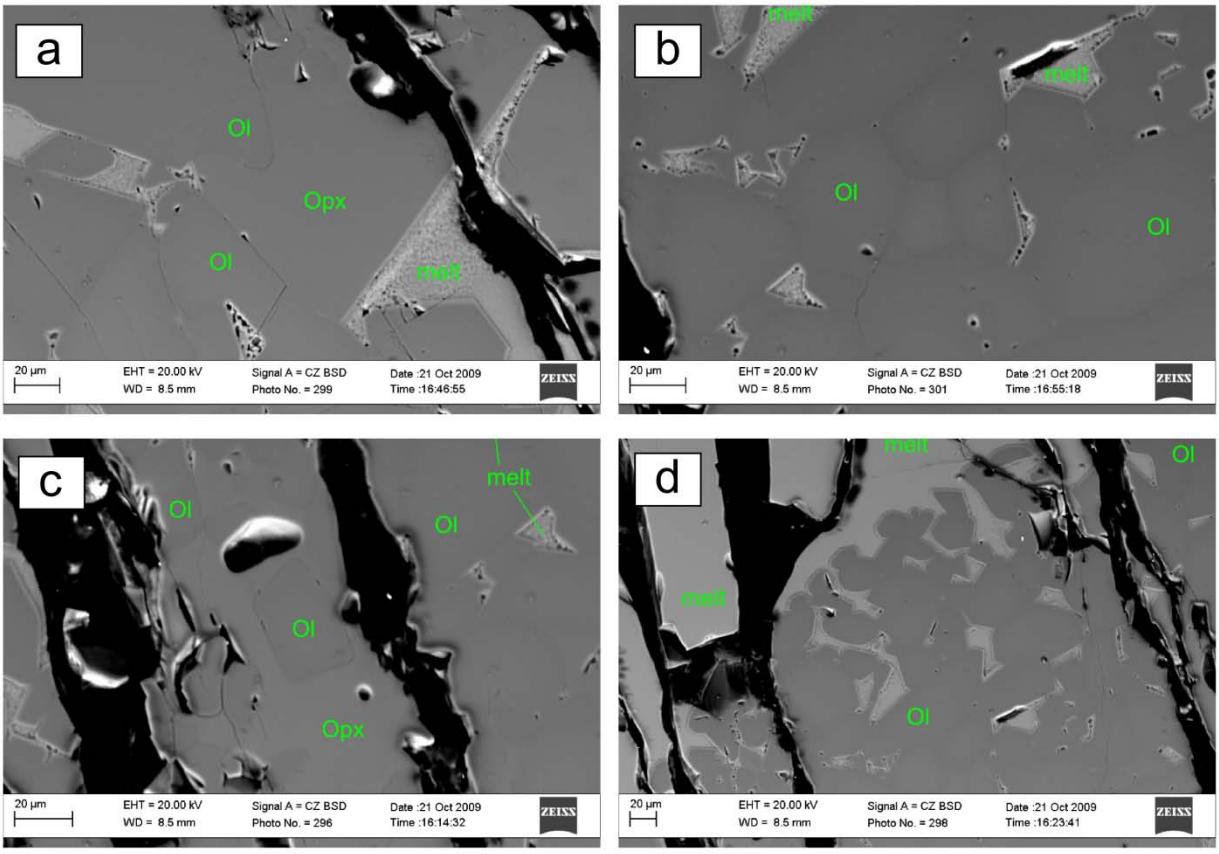

Appendix 3.4: Back-scattered electron images of experiment DK4 (2.5 GPa, 1100°C).

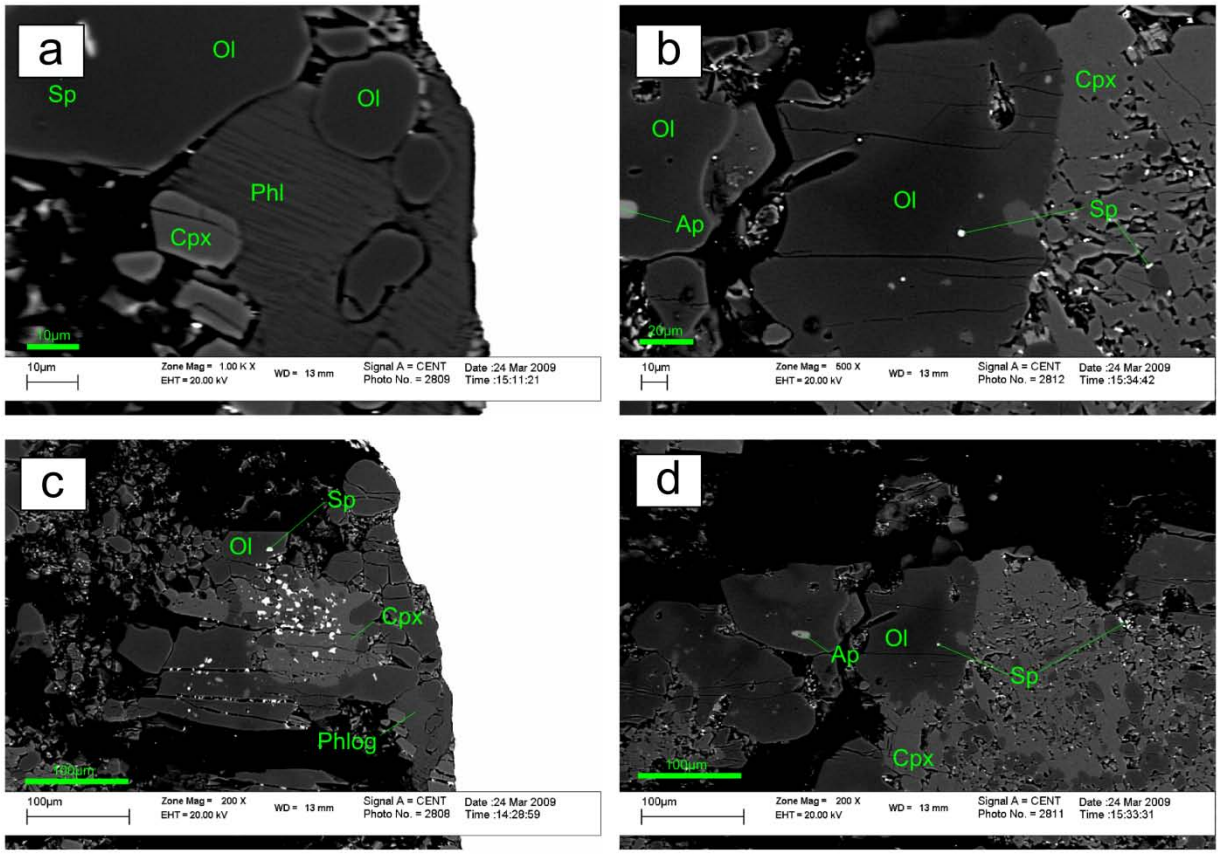

Appendix 3.5: Back-scattered electron images of experiment DK3 (2.5 GPa, 1200°C).

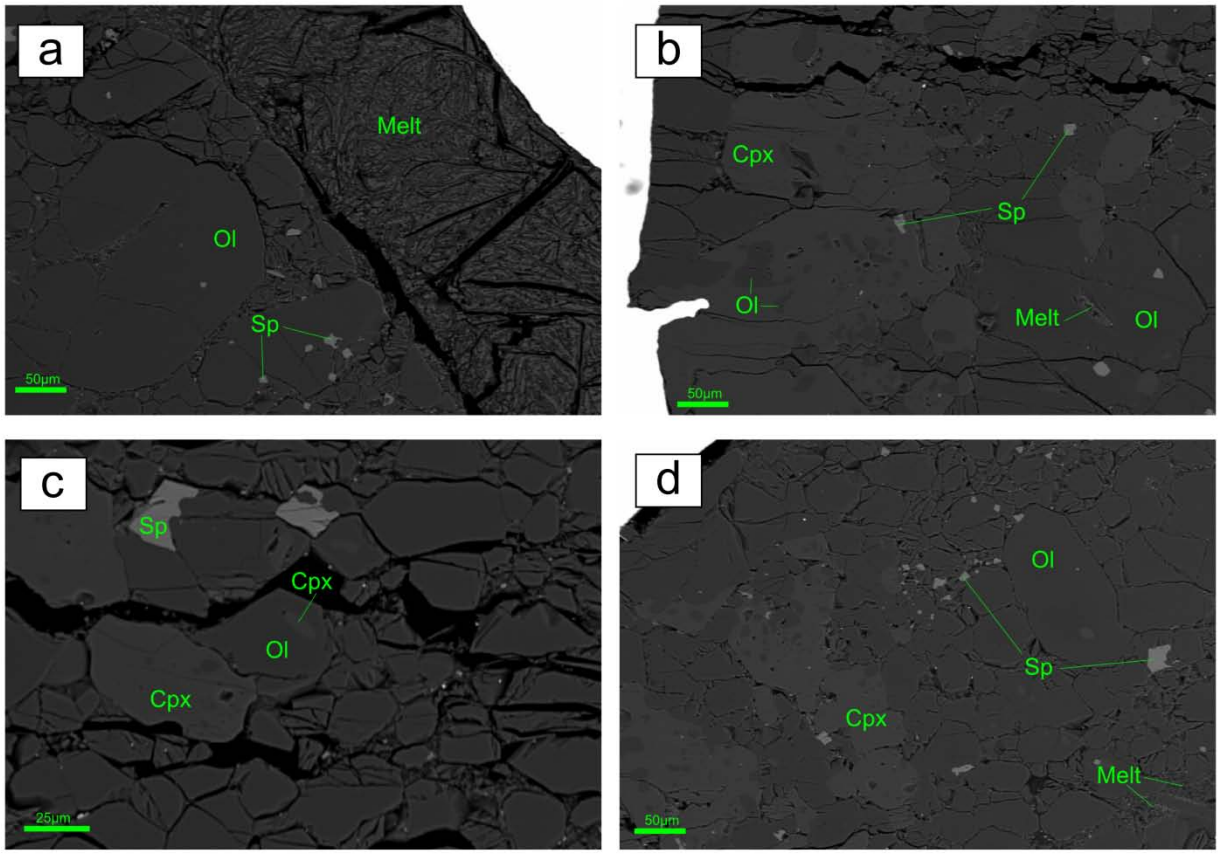

Appendix 3.6: Back-scattered electron images of experiment DK12 (2.5 GPa, 1300°C).

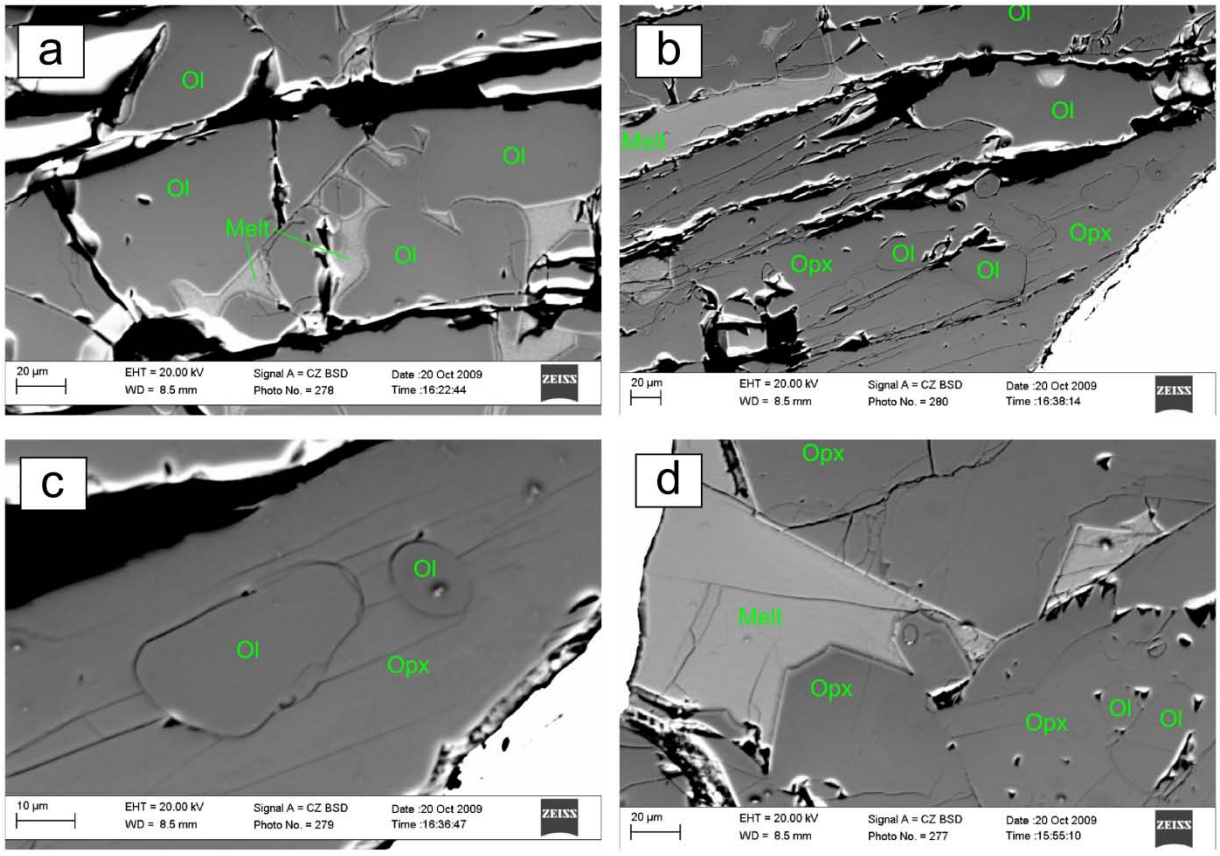

Appendix 3.7: Back-scattered electron images of experiment DK15 (3.0 GPa, 1100°C).

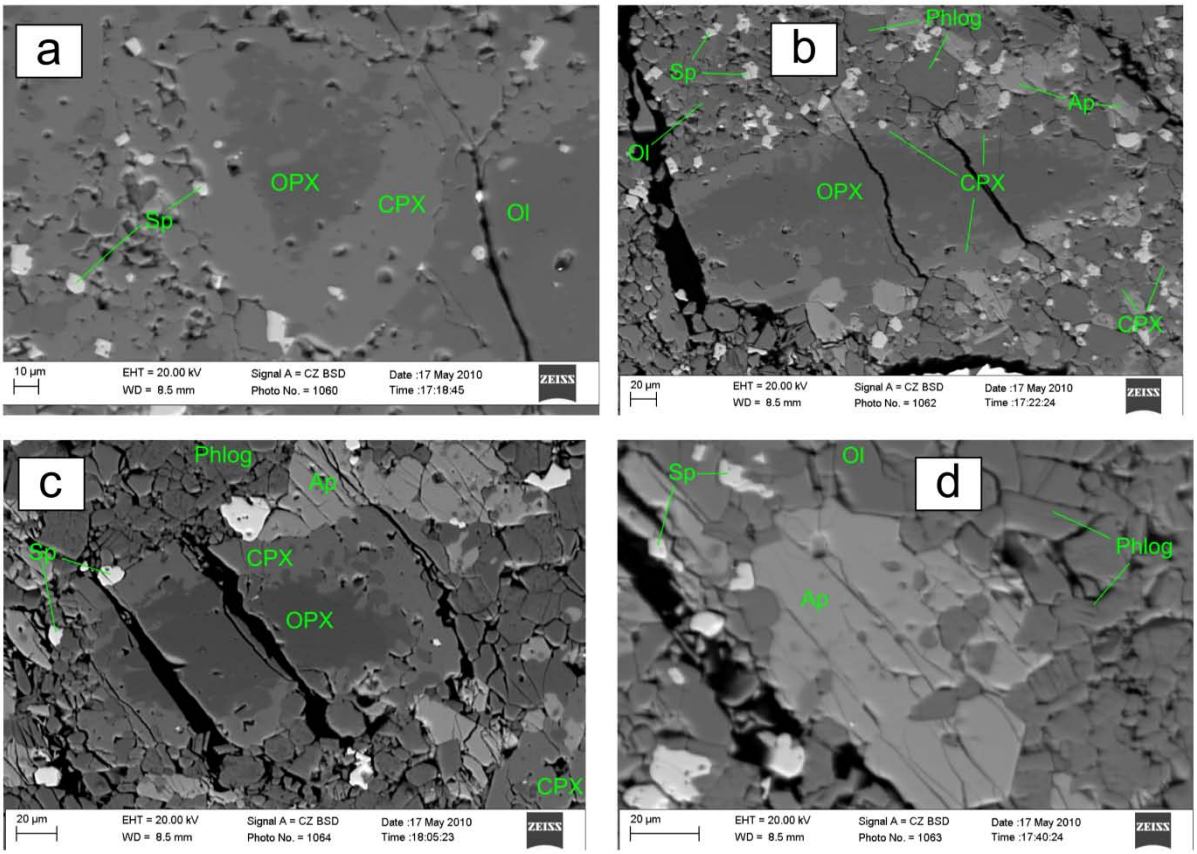

Appendix 3.8: Back-scattered electron images of experiment DK16 (3.0 GPa, 1200°C).

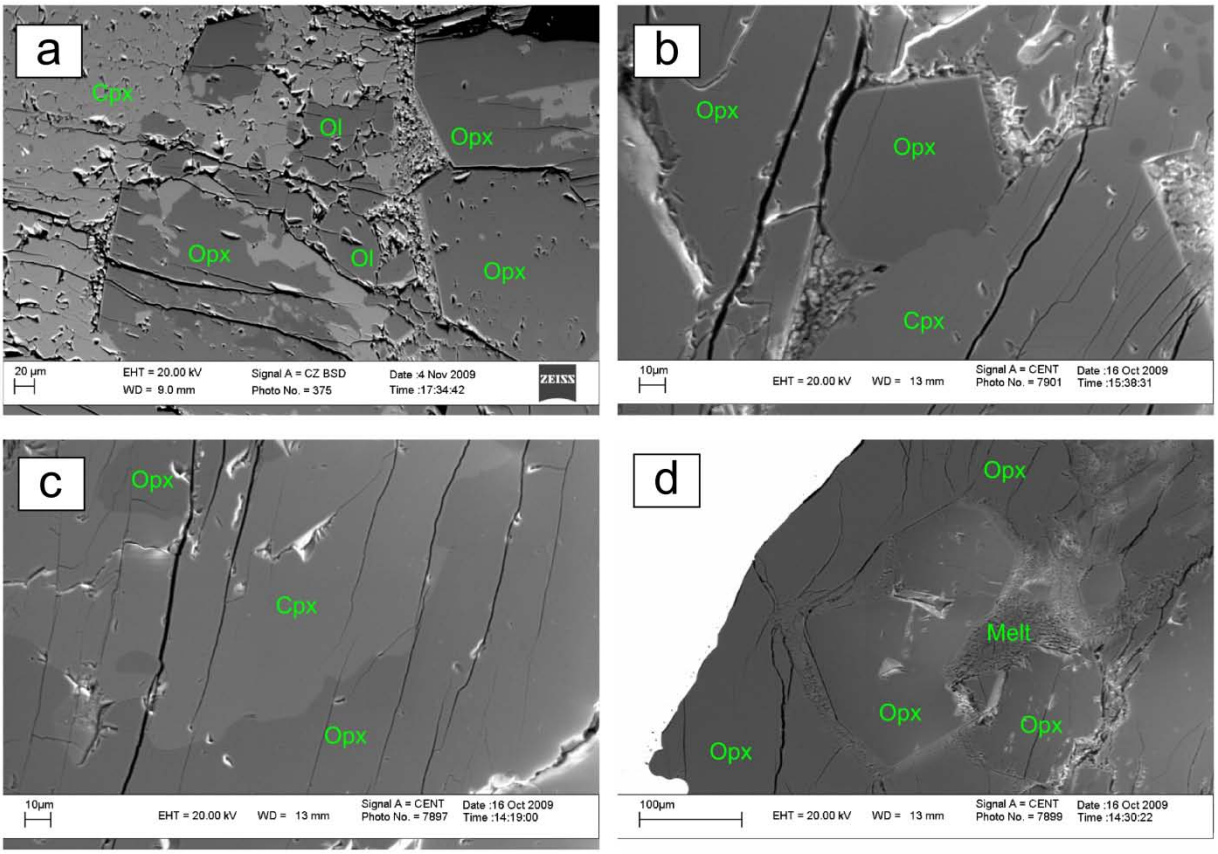

Appendix 3.9: Back-scattered electron images of experiment DK13 (3.0 GPa, 1300°C).

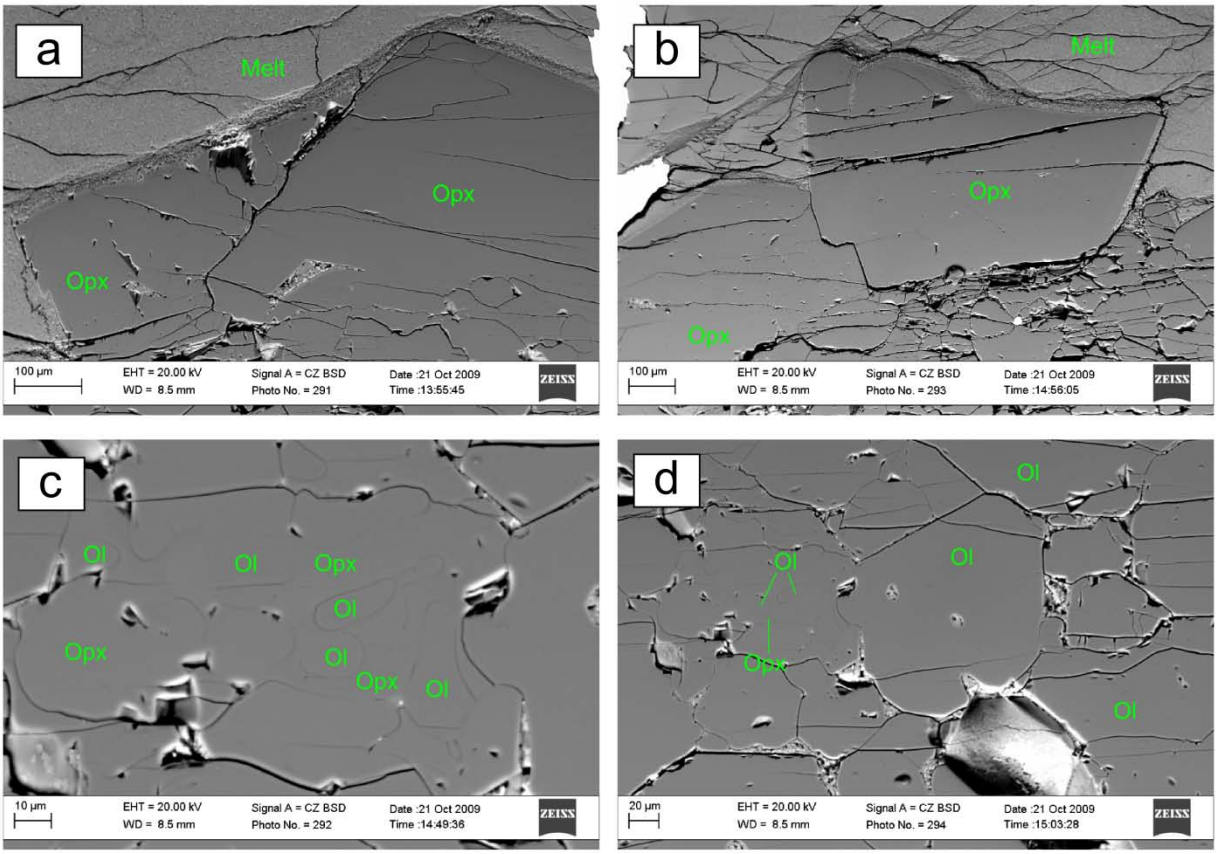

Appendix 3.10: Back-scattered electron images of experiment DK19 (3.5 GPa, 1100°C).

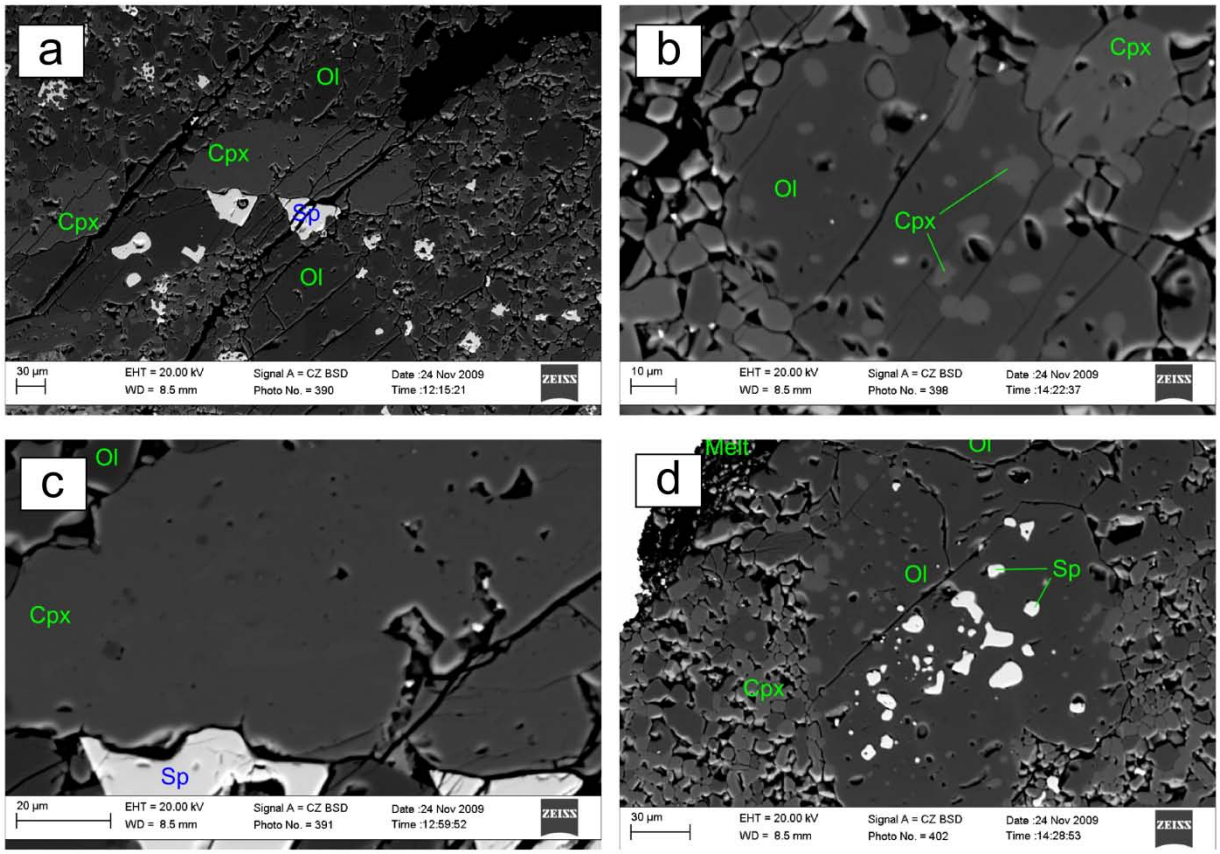

Appendix 3.11: Back-scattered electron images of experiment DK18 (3.5 GPa, 1200°C).

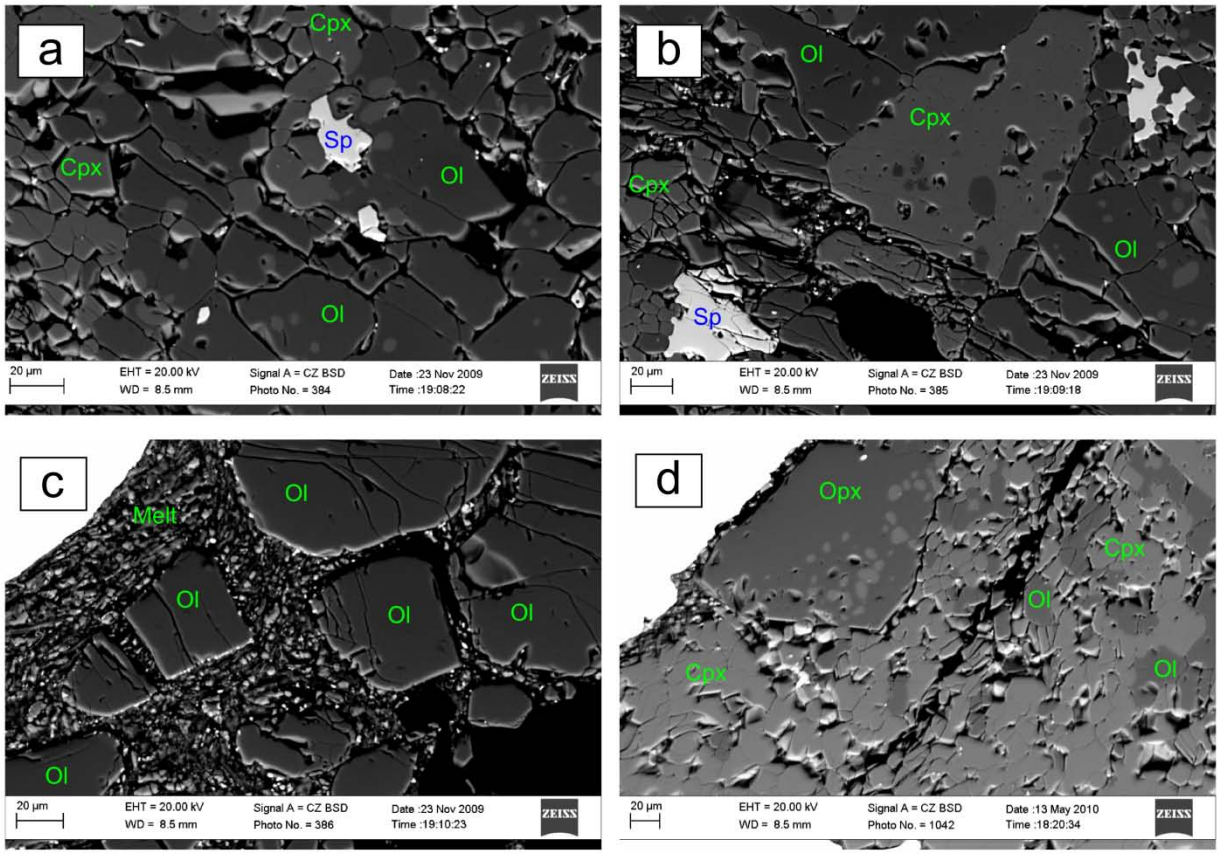

Appendix 3.12: Back-scattered electron images of experiment DK17 (3.5 GPa, 1300°C).